A Novel Time-Interval Based Modulation for Large-Scale, Low-Power, Wide-Area-Networks

YAMAN SANGAR, YOGANAND BIRADAVOLU, and BHUVANA KRISHNASWAMY,
University of Wisconsin-Madison

Wireless communication over long distances has become the bottleneck for battery-powered, large-scale deployments. Low-power protocols like Zigbee and Bluetooth Low Energy have limited communication range, whereas long-range communication strategies like cellular and satellite networks are power-hungry. Technologies that use narrow-band communication like LoRa, SigFox, and NB-IoT have low spectral efficiency, leading to scalability issues. The goal of this work is to develop a communication framework that is energy efficient, long-range, and scalable. We propose, design, and prototype WiChronos, a communication paradigm that encodes information in the time interval between two narrowband symbols to drastically reduce the energy consumption in a wide area network with large number of senders. We leverage the low data-rate and relaxed latency requirements of such applications to achieve the desired features identified above. We design and implement chirp spread spectrum transmitter and receiver using off-the-shelf components to send the narrowband symbols. Based on our prototype, WiChronos achieves an impressive 60% improvement in battery life compared to state-of-the-art LPWAN technologies in transmission of payloads less than 10 bytes at experimentally verified distances of over 4 km. We also show that more than 1,000 WiChronos senders can co-exist with less than 5% collision probability under low traffic conditions.

CCS Concepts: • **Hardware** → **Wireless devices**; • **Networks** → *Cross-layer protocols*; **Link-layer protocols;**

Additional Key Words and Phrases: Low-power wireless, timing interval modulation, scalability

ACM Reference format:
Yaman Sangar, Yoganand Biradavolu, and Bhuvana Krishnaswamy. 2022. A Novel Time-Interval Based Modulation for Large-Scale, Low-Power, Wide-Area-Networks. *ACM Trans. Sensor Netw.* 18, 4, Article 68 (November 2022), 30 pages.
https://doi.org/10.1145/3549543

1 INTRODUCTION

Wireless data delivery is key to real-time data collection and analysis in the fast-growing areas of smart agriculture [1, 2], livestock monitoring [3], and precision farming [4]. Large-scale soil monitoring networks currently use cellular and satellite networks to collect real-time data over a long period of time [5]. Real-time data collection from in-situ sensors in fields throughout the crop season will provide an understanding of the spatio-temporal dynamics of environmental factors

Yaman Sangar and Yoganand Biradavolu contributed equally to this research.
Authors' address: Y. Sangar, Y. Biradavolu, and B. Krishnaswamy, University of Wisconsin-Madison, Madison, WI 53706; emails: {sangar, ybiradavolu}@wisc.edu, bhuvana@ece.wisc.edu.

1550-4859/2022/11-ART68 $15.00
https://doi.org/10.1145/3549543

Table 1. Comparison of Current Wireless Technologies and WiChronos

Technologies	Reported Range	Battery Life (>1 yr)	Scalable (>100)	Data-rate (kbps)
WiFi	<200 m	X	✓	<54k
Cellular	<1 km	X	✓	<10k
BLE	<100 m	✓	X	<2k
Zigbee	<1 km	✓	X	<250
Passive RFID [10]	<10 m	✓	X	<40
Active RFID [11]	<100 m	✓	X	<40
AmbientBackscatter [12]	0.7 m	✓	X	<1
LoRaBackscatter [13]	2.8 km – 5 m	✓	X	.05 – 37.5
pLoRa [14]	1.1 km	✓	X	<.0002
LoRa	<15 km	✓	X	<50
SigFox	<10 km	✓	X	<.1
WiChronos	32 km Expt: 4 km	✓	✓	<1

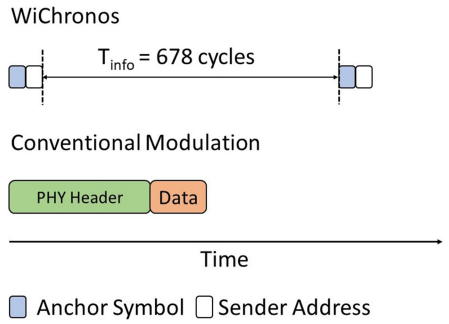

Fig. 1. An illustration of WiChronos.

and various chemical and biological processes in the soil, which can, in turn, be used to improve soil health and crop growth. However, due to the high infrastructure costs for solar panels and batteries to enable wireless information retrieval, monitoring sensor networks are deployed only at limited locations and have latencies ranging from one day up to one month [5, 6]. Such monitoring systems typically deploy sensors in large fields and share the following requirements: (1) Long battery life, (2) Long-range communication to reduce infrastructure costs, (3) Scalability and co-existence, and (4) Low cost, with less stringent demands on data rate, latency, and payload size compared to traditional networks. For example, sensors used to measure soil moisture, the chemical and biological properties of soil typically have a resolution of 8–12 bits [7–9], offering a light payload. Also, the gradual change in the rate of these parameters results in reduced demands for data-rate and latency. However, the monitoring systems are often deployed in harsh, remote environments on a massive scale and are expected to have battery life in the order of years.

Current energy-efficient protocols such as Zigbee [15], **Bluetooth Low Energy** (**BLE**) [16], and backscattering [12–14, 17] consume less than 50 mW power during active transmission, allowing for a long battery life. However, their communication range is on the order of 10s of meters, and they require infrastructure support for coverage. On the other hand, approaches for long range such as cellular and satellite networks are expensive and energy consuming, limiting the battery life and scalability of the system. In Table 1, we compare the communication range, battery life, data-rate, and ability to support more than 100 nodes in a network of state-of-the-art wireless technologies. *Evidently, existing strategies for addressing low-power and long-range do not co-exist efficiently in a large-scale network.* This inefficiency can be explained by the impact of **bandwidth** (**BW**) on energy consumption, communication range, and network capacity. In an **additive white Gaussian noise** (**AWGN**) channel, the network capacity or maximum channel data-rate is given by

$$C = B \log_2 \left(1 + \frac{S}{N_0 B}\right), \tag{1}$$

where B is the bandwidth in Hz, S is the signal power, and N_0 is the noise spectral density [18]. A wideband signal can achieve a high data-rate, in turn, reducing the time-on-air (the amount of time a channel is occupied). With reduced time-on-air, the active transmit time of the RF module decreases, reducing energy consumption. However, the signal-to-noise ratio $SNR = \frac{S}{N_0 B}$, decreases with an increase in BW, since the noise power increases with BW. At long distances, the received signal power decreases due to path loss; hence a lower BW can decrease noise power and increase

the SNR. Therefore, a **narrowband** (**NB**) signal is more suitable for communication over long distances. In summary,

$$\texttt{Energy} \propto \texttt{Time-on-air} \propto \frac{1}{B}, \quad \texttt{Range} \propto \frac{1}{B}, \quad \texttt{Scale} \propto B.$$

The above conflicting requirement on BW makes it challenging for low-power and long-range solutions to co-exist. In other words, the existing technologies do not satisfy all the three requirements we identified: low-power, long range, and network scalability. **Low Power Wide Area Network** (**LPWAN**) technologies such as LoRa [19], SigFox [20], NB-IoT [21] have been successful in achieving long range [22, 23] and long battery life by limiting the *duty-cycle* (the fraction of time during which a node is in active transmit or receive mode): reducing the number of messages per day. Recent works such as LMAC [24], FREE [25] aim to use CSMA-based approach to improve network scalability. While CSMA reduces collisions, the need for carrier sensing draws additional current, in turn, increases the energy consumption. Use of transmission buffers is only effective for higher payloads which are not the target applications for WiChronos.

In other words, existing LPWAN solutions reduce the overall energy by limiting the airtime of each device in a day. They do not address the fundamental tradeoff between low power and long range. Therefore, as the network scales, their cumulative airtime will increase, leading to an increase in the probability of collisions, rendering them unsuitable for large-scale deployment.

In this work, we develop a communication framework that addresses the fundamental tradeoff between low power and long range in large-scale networks that have relaxed data-rate and latency requirements. *We propose WiChronos, a modulation technique that encodes information in the time interval between two NB symbols.* A WiChronos sender transmits exactly two *anchor* symbols per message, namely *preamble* and *postamble*, and the data modulates the duration between them. We leverage the low data-rate and small payload requirements of monitoring systems in agriculture, remote tracking, and derive benefits from the resources at the receiver to design energy-efficient transmitters. We further design a NB **Chirp Spread Spectrum** (**CSS**) modulation for optimum anchor symbol design to maximize the network scale, communication range, and battery-life requirements. We refer to a NB transmission as that where the transmit and receive BW are within few hundreds of kHz. Even though CSS is a spread spectrum modulation, since the BW of operation is below 100 kHz, we refer to it as NB. Thus, we use the term NB chirp in our implementation of CSS modulation. To the best of our knowledge, this is one of the first works to design and implement CSS modulation using off-the-shelf radio modules and microcontrollers. While wideband receiver will have a higher noise floor, chirps are inherently resilient to noise and can be detected and demodulated accurately in low SNR scenarios. Hence, WiChronos implemented with CSS modulated anchor symbols is able to achieve long communication range of over 4 km, while simultaneously offering long battery life and large-scale deployments.

WiChronos achieves **energy efficiency** by minimizing the number of symbols and (hence the time-on-air) per message, and **long range** by transmitting short CSS modulated anchor symbols over NB [26], that are resilient to interference. The reduced time-on-air and improved spectral efficiency allow the network to **scale better**. **WiChronos trades off data-rate to achieve the above three features.**

Figure 1 illustrates WiChronos and contrasts it with other modulations used in LPWANs. A WiChronos sender with a sensor data of 678 units transmits an anchor symbol (*preamble*), goes to sleep for 678 clock cycles (that corresponds to data), and wakes up to send another anchor symbol (*postamble*). The anchor symbols consist of a training sequence followed by a unique sender address. The sleep time encodes the entire message to be transmitted. The time-on-air of WiChronos is thus independent of the payload length (10 bits in this example) and only a function of the anchor symbols; by separating payload transmission from time-on-air, we reduce the impact of

BW on the time-on-air, without affecting the communication range. In the case of traditional modulations such as LoRa or SigFox, the data value of 678 is mapped to bits, which are then mapped to symbols for the corresponding modulation technique and transmitted over the air and hence the time-on-air is proportional to the payload length. Other time interval based modulations such as M-PPM transmit multiple pulses over air; the time slots in which the pulses are sent indicate the message.

To this end, we note that WiChronos is most suitable for applications with shorter payloads such as smart soil monitoring, food temperature monitoring, where frequent record of short data values are typical. When used in applications with larger payload, the time required to send the data increases, lowering the per-node throughput. We explore this limitation further in Section 9.

Toward implementing WiChronos in a wireless network, we identify the challenges in designing an optimal anchor symbol in terms of length, modulation parameters, and **medium access control** (**MAC**) in Section 4.2. We prototype WiChronos using inexpensive off-the-shelf radio modules and **microcontroller units** (**MCU**), using software-only changes. Based on our experimental implementation on MSP 430 [27], Linx-NT [28], CC1125 [29], and USRP B200 [30], we estimate an impressive battery life of over five years using a coin cell battery (250 mAh). We experimentally verify a range of over 4 km. Furthermore, we extrapolate the recorded SNR and show an estimated achievable range of 32 km. Also, we estimate the probability of collision to be less than 5% in a 1000-node network under low traffic conditions. To this end, we make the following contributions:

— We propose an energy-efficient modulation technique that encodes information in the time interval between two symbols, minimizing the number of symbols per message.
— We design and implement spectrally efficient, CSS modulated anchor symbols using general purpose off-the-shelf radio and MCUs with low-power clocks. We design a chirp demodulator on USRP B200 to receive anchor symbols.
— We implement an ALOHA-based MAC protocol and analyze its robustness to collisions in large-scale deployments, allowing the network to scale seamlessly.
— We prototype the proposed framework using off-the-shelf, low-cost RF modules and MCUs with low-power clocks.
— We prototype the proposed framework on different radios and experimentally show that WiChronos can reach distances of over 4 km and support multiple concurrent transmissions.

The remainder of this article is organized as follows. In Section 2, we provide background on the strategies for low power and long range, and motivate the need for a unifying algorithm in a large-scale network. In Section 4, we present the design and features of WiChronos, followed by a discussion on the challenges and throughput performance in Section 5. Experimental evaluation is presented in Section 7. Related work is discussed in Section 8. Finally, we identify the limitations and potential future work in Section 9 followed by our conclusions in Section 10.

2 BACKGROUND AND MOTIVATION

The overall power consumed by a sensor node is dominated by the communication module [31, 32]. Algorithms, protocols, and architectures have been developed to reduce the active transmit time and hence reduce the power consumption in the areas of **Wireless Sensor Networks** (**WSN**), AdHoc Networks, and Internet-of-Things. We broadly classify existing low power strategies for WSNs into the following five categories [4, 33–35]: (1) Duty Cycling, (2) Routing, (3) Data reduction, (4) Radio module optimization, and (5) Energy harvesting and backscatter.

Smart sleep/wake-up protocols [36, 37], event-triggered wake-up [38], and scheduled MAC protocols [39, 40] have been proposed to reduce the active transmit and/or receive time of the radio

transceiver. Though duty-cycling-based approaches reduce the power consumption of the overall network, they are still limited by the payload length. Data compression [41], prediction [42, 43], and cooperative communication [44, 45] techniques have been proposed to reduce the amount of data to be transmitted, which, in turn, reduces the energy per message. Network topology aware strategies have been developed to improve the lifetime of a sensor network through clustering [46], energy-aware routing [47], data gathering, and data forwarding [48]. These approaches decrease the overall energy consumption by leveraging the hierarchical topology and varying the energy constraints of nodes in the network [49, 50]. A new wave of battery-less sensors harvest energy from ambient signals and/or dedicated sources [12, 13] and use backscattering to communicate. However, these techniques are feasible only within a short range and require an additional signal source to piggyback on for long-range communication [13, 14]. Active and passive RFID tags [10, 11] are energy efficient but only work for a short range [51] and/or low traffic. RFIDs also are limited by the energy-range-scale tradeoff presented in Section 1.

The limited range of existing energy-efficient strategies can be attributed to the BW and propagation of RF signals. The range of an RF signal depends on the link budget (shown below) that accounts for the gains and the losses.

$$P_{Rx} = P_{Tx} + P_G - P_L, \tag{2}$$

where P_{Rx} is the received power, P_{Tx} is the transmit power, P_G accounts for the antenna gains, and P_L is the aggregate loss due to filter/cable attenuation, known experimental conditions, and path loss (P_{PL}). Free space path loss is given by

$$P_{PL} = -10 \log_{10} \frac{\lambda^2}{(4\pi d)^2} = 22dBm + 20 \log_{10} \frac{d}{\lambda}, \tag{3}$$

where d is the distance between the sender and the receiver, and λ is the wavelength. Radio optimization techniques to improve P_{Tx} such as directional antennas [39], Multiple-Input Multiple-Output, and mobility-based solutions such as Mobile Ad-Hoc Networks [52–54] are energy consuming and not suitable for low-power communication. Given the FCC limit on transmit power, the link budget depends on the path loss, which is inversely proportional to the wavelength (i.e., path loss increases with increasing frequency).

Existing technologies for long range such as cellular networks, NB-IoT, Sigfox, and LoRa operate in the sub-GHz bands to reduce path loss. Cellular and NB-IoT require high-complexity RF front end and LTE infrastructure for scheduling and synchronization [55]. SigFox and LoRa operate at lower BW to achieve long range, leading to an increase in the time-on-air. Similarly, Zigbee 3.0 [56] reduces data-rate and increases transmit power to improve range, in turn, increasing time-on-air. To achieve long battery life, LPWAN solutions limit the number of messages per day. Therefore, as the number of messages increases, the overall energy consumption increases, making them inefficient for an energy-constrained system. Also, with increasing scale, collision rate increases, which leads to a decrease in the network throughput [19–21].

To summarize, existing energy-efficient and long-range strategies cannot co-exist in a large-scale network. In this work, we develop a communication framework for real-time monitoring system that is energy-efficient, communicates over long distances, and supports a large number of nodes.

3 A PRIMER ON CSS MODULATION

In this work, we propose a CSS modulation to transmit the anchor symbols. Chirp is a signal whose frequency varies with time. Chirps are found in nature, used by birds and aquatic life for localization, and in Radar [57] for ranging. CSS modulation has been recently used by LoRa to improve communication range and be resilient to interference. In CSS, the data modulates the

starting frequency of a chirp signal. The gradient of the linear chirp determines the chirp duration and the rate of chirp transmission. A linear chirp symbol $S_i(t)$ of duration T whose frequency increases from −BW/2 to BW/2 with an initial frequency f_i and gradient $k = \frac{BW}{T}$ is given by

$$S_i(t) = S(t) \cdot e^{j2\pi f_i t} \qquad S(t) = e^{j2\pi\left(\frac{-BW}{2} + \frac{kt}{2}\right)t} \tag{4}$$

where $S(t)$ is the baseline up chirp. Any data symbol $S_i(t)$ is obtained by shifting the baseline up chirp $S(t)$ in time domain. Any time offset or timeshift of a chirp signal translates to frequency offset. LoRa uses CSS modulation to transmit data; WiChronos, on the other hand, uses CSS to modulate only the anchor symbols.

CSS demodulation is performed by multiplying the received chirp with the complex conjugate of the up chirp (Equation (5)). Performing Fourier Transform of this resulting signal will result in a peak at the unique starting frequency.

$$S_i(t)S^*(t) = e^{j2\pi f_i t}. \tag{5}$$

4 AN OVERVIEW OF WICHRONOS

In the majority of the digital modulation techniques used in wireless networks, data modulates the characteristics of the carrier signal [58]. For example, 2-FSK maps bit 0 and bit 1 to two distinct frequencies, transmitting 1 bit per symbol. The total number of symbols per message, therefore, depends on the modulation technique and the message length. Higher-order modulation techniques such as 64-QAM can encode more bits per symbol, but have larger energy per bit, E_b while lower-order modulations such as 2-FSK have lower E_b but an increased number of symbols per message.

A modulation technique that reduces the number of symbols per message without increasing E_b is required to achieve energy efficiency. With this insight, we propose WiChronos, a modulation technique that encodes information in the time interval between two anchor symbols. Figure 1 illustrates an example with an integer data 678 from a 10-bit sensor. The transmitter sends a predefined preamble and waits for 678 clock cycles and then a predefined postamble. The receiver, with a priori knowledge of the anchor symbols of each transmitter, identifies the sender from the preamble and triggers the corresponding timer to start (or stop) on the reception of the preamble (or postamble). In the absence of any timing errors and prior knowledge of clock rate, the number of clock cycles counted at the receiver is equal to that at the transmitter. Therefore, irrespective of the data to be transmitted, WiChronos sends two anchor symbols per data.

Thus, the total number of symbols transmitted on-air and the energy consumed by the RF module depends only on the length of the anchor symbols and is not affected by the length of the sensor output (10-bits in this example). WiChronos hence satisfies the two requirements identified earlier for energy-efficient modulation, i.e., (1) Minimum number of symbols, (2) Non-increasing energy per bit E_b. In the rest of this section, we discuss the challenges in achieving the promise of WiChronos and propose solutions to address them.

4.1 Energy Efficiency

A key insight for the energy-efficient design of WiChronos is that the RF module is the bottleneck of a sensor node [32]. Energy consumed by a sensor node is given by $V \cdot I \cdot \delta t$, where V is the voltage, I the average current drawn for a duration δt. For a constant V and given δt, the current drawn, which determines the energy consumption can be classified into six categories as

(1) I_{a-u}: Active - MCU
(2) I_{s-u}: Sleep - MCU
(3) I_{i-rf}: Idle - RF module
(4) I_{s-rf}: Sleep - RF module
(5) I_{r-rf}: Active listen - RF module
(6) I_{t-rf}: Active transmit - RF module

Table 2. Current Consumption of Individual Modules

		Active Current (mA)	Idle Current (mA)	Sleep Current (nA)
MCU	MSP430 [59]	1	0.7	45
	STM32L [60]	0.45	0.3	140
Tx	Linx-NT [28]	42.5	42.5	1
	CC1101 [61]	27.4	27.4	200
Rx	Linx-NT	22.5	22.5	1
	CC1101	15.4	15.4	200

Table 2 enumerates the above currents for selected OTS hardware. The active and sleep currents of MCUs are few mA and μA, respectively, as noted in row 2 of Table 2. I_{t-rf} depends on the transmit power of the RF module and the protocols implemented in the transceiver. The active currents of RF module are on the order of tens of mA. Therefore, an energy-efficient transmitter must minimize the amount of time spent in active mode. By encoding information in the time interval between symbols, we reduce the active transmit time of the RF module and the MCU. The energy consumption is further reduced by operating the MCU and the RF module in sleep mode during clock counting.

Figure 2 details our implementation in MSP430 FR2355. On reading analog data from the sensor, the transmitter converts it to a digital value (D), maps to clock cycles T_{info} (with redundancy to correct for timing errors), and sets TimerA to T_{info}. The MCU triggers the RF module to send a preamble and then set the RF to sleep. The MCU itself goes to sleep mode, with TimerA running in the background. After T_{info} cycles, TimerA interrupts the MCU to turn on the RF to send postamble. Since T_{info} is the time *difference* between the symbols, the transmitter and receiver clocks need not be synchronized. It is sufficient to use the same clock rate. Since the RF and MCU modules are in sleep mode during data transmission (T_{info}), the overall energy consumption is unaffected by the message length. The energy consumption of data transmission is

$$\mathrm{E} = V\,(I_{a-u} + I_{t-rf})\,2t_{anchor} + V\,(I_{s-u} + I_{s-rf})\,T_{info} \tag{6}$$

where t_{anchor} denotes the duration of anchor symbols. The overall energy consumption is therefore determined by the modulation parameters used to transmit the anchor symbols, the anchor symbol length, and the corresponding current drawn. Optimum anchor symbol length is crucial to achieving the promised energy efficiency.

4.2 Anchor Symbol Design

Predefined preambles are commonly used in communication systems to indicate the start of a packet and to achieve frame (and/or bit) synchronization [58]. The anchor symbols play the same role; indicate the start of a message (to start and stop clock counting) and assist the receiver to identify the sender. Since we specifically focus on networks with relaxed data-rate requirements, the anchor symbols are transmitted at the order of few kilobits per second over narrow BW. At such low data-rates, the time and the number of bits required for the **Automatic Gain Control** (**AGC**) in the RF front end to settle, is reduced. Furthermore, UNB communication requires much shorter preamble than coded modulations [62]. For example, TI CC1125 [29] uses an AGC design with a 4-bit settling time along with smart carrier sensing to reduce false positives. The lower bound on the anchor symbol length is thus determined by the RF front end and the modulation parameters. In order to differentiate between the start counting and stop counting triggers, each sender is assigned two unique addresses, i.e., each sender has a unique preamble and postamble.

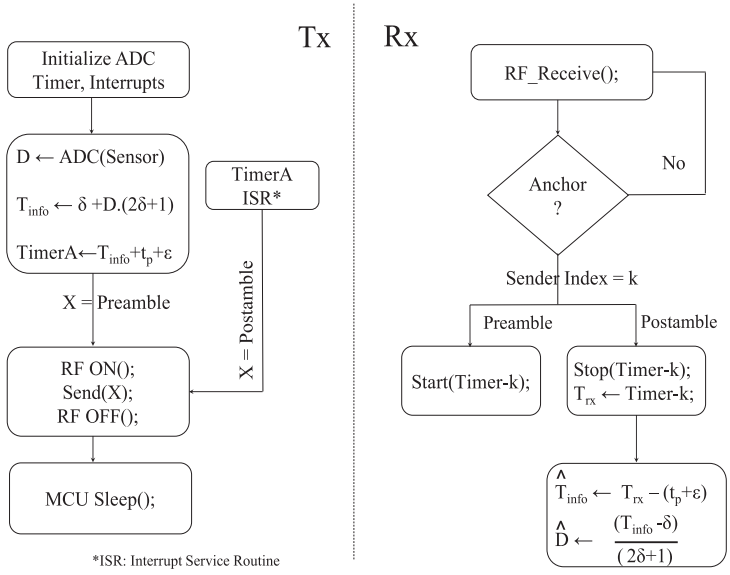

Fig. 2. System implementation flow diagram of WiChronos on MSP430.

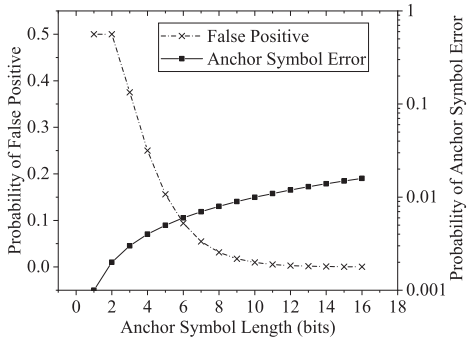

Fig. 3. FSK Anchor symbol length design.

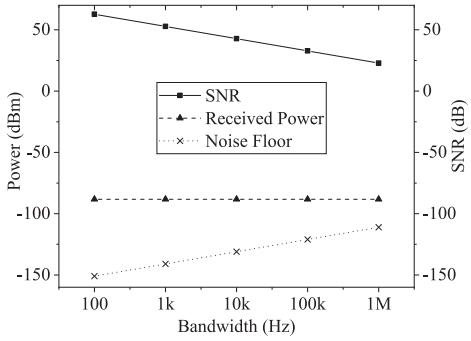

Fig. 4. Impact of BW on receiver sensitivity.

We propose and analyze the effectiveness of two anchor symbol modulations: (1) Ultra NB FSK and (2) NB CSS.

We define the optimum anchor symbol length to be the shortest length that enables reliable decoding at the receiver, i.e., it must minimize the probability of error in decoding and has a low false-positive rate. For a given modulation, SNR, and the corresponding BER p_b, the probability of symbol error and false-positive are

$$P_e = \sum_{k=0}^{e} \binom{N}{k} \cdot {p_b}^k q^{N-k}, \qquad P_f = (0.5)^N \sum_{i=0}^{\epsilon} \binom{N}{i}, \tag{7}$$

where e is the maximum number of bit errors that can be tolerated by the receiver for an N-bit anchor symbol. Figure 3 plots the above probability of symbol error P_e and probability of false positive P_f as a function of anchor symbol length for e = 0. P_e increases with symbol length; therefore, shorter anchors are desirable to reduce symbol error while P_f decreases with symbol length. With

short symbols, the probability of a random bit pattern from other devices or interference being falsely detected as the anchor is high. We identify the smallest anchor symbol length that renders low P_f and P_e for a given anchor symbol modulation, expected SNR, desired false positive rate, and symbol error rate.

4.2.1 FSK Modulated Anchor Symbol. First, we consider an FSK modulated anchor symbol and identify the optimum symbol length for WiChronos. We use BFSK to modulate the anchor symbols with an SNR $\geq$ 10dB, BER of $\leq 10^{-3}$. We choose 10-bit anchor symbol to achieve $P_f \leq 0.01$ and $P_e \leq 0.001$. It must be noted that this shortest anchor symbol length is required to transmit each *pulse* in any variant of PPM. The anchor symbol length calculation is unaffected by the receiver since we leverage the resource asymmetry in infrastructure mode and let the receiver to always be in *listen* mode. The minimum anchor symbol length is determined by the settling time of the RF module, the probability of false positives, and the probability of symbol error. RF modules with advanced carrier sensing and AGC can further reduce the settling time and false positives, leading to shorter anchor symbols. As the number of transmitters increases, the number of unique addresses and hence the length of the anchor symbol will increase, inversely affecting the energy efficiency (more details in Section 4.4).

4.2.2 CSS Modulated Anchor Symbol. In order to overcome the scalability challenge of UNB-FSK modulation, we propose a CSS modulated anchor symbol design. As discussed in Section 3, a chirp is a signal whose frequency varies with time. We design a linear CSS modulation to maximize the number of unique anchor symbols that can be assigned without compromising the energy consumption of the transmitter. While FSK uses one frequency per symbol, CSS uses the entire BW for each chirp. Such a spread spectrum approach is resilient to channel noise and interference, in turn, resulting in fewer false positives than FSK. Furthermore, CSS is resistant to multi-path interference even when operating in low power. On the contrary, multipath fading from reflection, scattering from buildings, hills, and diffraction have a negative effect on the bit error rate of an FSK modulated anchor symbol.

We define C_i to be a chirp symbol whose initial frequency is f_i. The frequency of C_i increases linearly from f_i to BW and back to f_i in one symbol duration. The difference between two consecutive frequencies in a chirp is f_{step} and will be referred to as the step size of the chirp. This step size is determined by the RF front end and hence is limited by the hardware. Therefore, the number of unique chirps, N_{chirp} is determined by $\frac{BW}{f_{step}}$. The duration of a chirp symbol is determined by the hardware and is lower bounded by $\frac{1}{BW}$, where BW is the transmit BW of the chirp symbol.

Since CSS has inherently low false-positive rate, we define the optimum CSS anchor symbol length as the shortest length that can be decoded with a low probability of error. We illustrate our proposed anchor symbol design in Figure 5, where each sender is assigned two unique sequence of chirp symbols. For example, the start anchor of Sender 1 is C_1, C_2, C_3, C_4 and that of Sender 2 is C_1, C_2, C_3, C_5.

During the transmission of a chirp, the signal and noise are spread over the entire BW. Upon demodulation, the receiver despreads the signal, during which the signal power concentrates at a singular FFT peak as described in Section 3. Chirp demodulation relies on the receiver demodulation window to be perfectly aligned in time with the chirp signal. To facilitate this synchronization and accurate detection of the start of the anchor symbols, we design an anchor symbol to consist of four up-chirps (C_0) that form the preamble, followed by a sequence of C chirp symbols that uniquely identify the transmitter. Each of these chirp symbols can be one of the chirps $C_1, C_2, \ldots, C_{N_{chirp}-1}$, where N_{chirp} denotes the maximum number of unique chirps that can generated. C_0 is dedicated for the preamble. Assigning two unique anchor symbols per transmitter, the

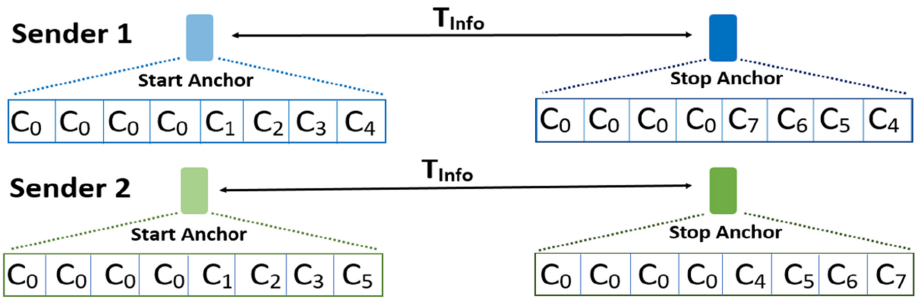

Fig. 5. WiChronos illustration with CSS Modulation for anchor symbols. Anchor symbol format is also illsutrated.

total number of transmitters that can be supported, $N_{transmitters}$, is calculated as

$$N_{transmitters} \leq \frac{(N_{chirp} - 1)^C}{2}. \tag{8}$$

In the example illustration in Figure 5, $C = 4, N_{chirp} = 8$. Therefore, for a given network scale, we determine the minimum anchor symbol length to be the smallest value of C that satisfies the above inequality. Network scale can be improved by increasing the BW, increasing number of chirp symbols, C, or number of unique chirps N_{chirp}.

4.3 Long-Range Communication

The second challenge identified in this work is achieving long range within the energy constraints. As discussed in Section 2, propagation loss is directly proportional to the distance and the frequency of operation. Following the IEEE 802.11ah standard [63], we operate in the sub-GHz spectrum and **narrow bandwidth** (**NB**) for long range. The range also depends on the *receiver sensitivity* (the minimum received power required to demodulate the signal with an acceptable BER), a characteristic of the receiver. For a given propagation channel and frequency of operation, the received power is obtained from Equation (2). SNR at the receiver depends on the received power and the noise floor, which is given by

$$\text{Noise floor} = -174 + NF + 10 \log_{10} BW. \tag{9}$$

Here, NF is the noise figure (the ratio of input SNR to output SNR at the receiver) and BW is the receiver BW [39]. Figure 4 shows SNR and NF as a function of BW. For a given received power, the noise floor increases with receiver BW, in turn, decreasing the SNR and the receiver sensitivity. NB and UNB modulations are capable of long range due to their improved receiver sensitivity and SNR from reduced BW. However, decreasing the receiver BW implies reduced transmit BW, leading to an increase in time-on-air and energy consumption. Thus, even in low data-rate applications, wireless systems operate at higher data-rates to save battery life. To overcome the impact of narrow BW, existing LPWAN strategies limit the number of messages to reduce the total *time-on-air* [64].

4.3.1 FSK Modulated Anchor Symbol. Due to its inherently reduced time-on-air, WiChronos can operate in UNB without significantly increasing the energy consumption. The increase in time-on-air from UNB transmission of the anchor symbols is much smaller than that of the entire message (as in other LPWAN techniques). In our evaluation, we modulate the anchor symbols using BFSK in the 902–928 MHz spectrum with a BW ranging from 10 kHz to 120 kHz. Operating at the 902–928 MHz spectrum also offers the advantage of mitigating multipath reflections and wideband interference. Devices operating in NB and UNB are unaffected by multipath as they experience no

inter symbol interference [65, 66]. This is a physical layer phenomenon and we discuss this in our future work as an area of further analysis.

4.3.2 CSS Modulated Anchor Symbol. The communication range for a given BW can be further improved by leveraging the spread spectrum gain provided CSS modulation. Due to its resilience to noise and interference, CSS offers an improvement in SNR for the same BW. In time domain, a chirp has signal power spread across the BW. When it is converted to frequency domain and multiplied with a down chirp, all the signal power that was spread across the BW concentrates at one frequency peak. This gain is inherent to CSS and is referred to as the spread spectrum processing gain. The processing gain is the ratio of the spread spectrum BW to the baseband BW. Compared to FSK using the same hardware, the processing gain from CSS increases the SNR and hence the range, with no impact on the system scale or energy consumption.

4.4 Medium Access Control

The third challenge identified in this work is that of **co-existence** in a large-scale deployment. In spite of the vast research on MAC protocols for large-scale [37, 67], ALOHA-based algorithms are implemented in LPWANs due to its simplicity. ALOHA allows a sender to transmit whenever it has data without any coordination between the senders. The simplicity of ALOHA makes it vulnerable to collisions in large-scale and/or heavy-traffic deployments. A packet collision occurs if one sender begins transmission during an on-going transmission, i.e., twice the data transmission period is *vulnerable* to collisions. LPWANs using ALOHA-based MAC protocols suffer from collisions in large-scale networks when the channel is used for transmission more than 20% of the time (on average) [58].

WiChronos (by design) has low time-on-air and leverages the simplicity of ALOHA without getting penalized by collisions. **Data transmission time and time-on-air are different for WiChronos, unlike existing digital modulations.** As shown in Figure 8, in current systems, the entire transmission is vulnerable to collisions, whereas, in WiChronos, only the anchor symbols are vulnerable, decreasing the probability of collisions. During the *data* transmission of one sender (T_{info}), the other sender can transmit their anchor symbols without affecting the on-going transmissions. We derive the probability of collisions given a node is transmitting a message following the textbook approach used in the analysis of ALOHA [68]. We assume a Poisson arrival process with a cumulative arrival rate of λ. Given a sender started a transmission, the event is a success if no other anchor is sent within $2t_{anchor}$.

$$\begin{aligned} \Pr(collision) &= 1 - \Pr(\text{no other event in } 2T') \\ &= 1 - e^{-\lambda 2T'}, \texttt{where T'} = t_{anchor} \end{aligned} \tag{10}$$

Figure 6 plots the probability of collision for a given node *transmitting a 1-byte message every 10 minutes* as a function of the network size. For SigFox, we assume its default overhead of 11 bytes at a data-rate of 600 bps. For LoRa, we assume the shortest preamble allowed with a **spreading factor** (**SF**) of 7, code rate 4/5, and 125 kHz BW [69], operating in implicit header mode without CRC. We turn off CRC and MAC overheads, as well as ACKs in LoRa for a fair comparison. An arrival rate of 2λ is used in the calculation for WiChronos to account for the two FSK modulated anchor symbols at BWs normalized to SigFox and LoRa.

4.4.1 FSK Modulated Anchor Symbol. With an increase in the number of transmitters, the probability of collision for SigFox is the highest among compared technologies, due to its very low data-rate and very high time-on-air. The above parameters for LoRa are chosen for low power and do not offer long range. For longer range, LoRa recommends higher SF, which will lead to

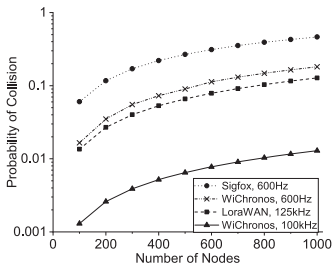

Fig. 6. Probability of collisions for SigFox, LoRa, and FSK-modulated WiChronos under varying BW.

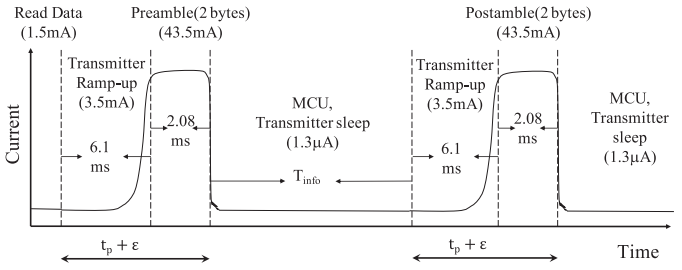

Fig. 7. Timing components of WiChronos sender.

increased time-on-air, thus increasing the probability of collision. The rate of increase of probability of collisions with network scale is slower for WiChronos due to its reduced air-time. *It can achieve energy efficiency without limiting the number of messages and/or the network size.* As shown in Figure 6, reducing BW (from 100 kHz to 600 Hz) increases the probability of collision due to increase in symbol duration. However, this increase in collision is smaller for WiChronos as only the anchor symbol duration contributes to collision as opposed to SigFox or LoRa where the entire payload increases the collision probability. Therefore, we can leverage NB and UNB to improve range without significantly affecting scalability and energy efficiency. In a network of 1,000 nodes, the probability of collision for SigFox and LoRa are 46.3% and 12.75% compared to WiChronos at 1.2% for a BW of 100 kHz and 1.8% for 600 Hz.

With increasing network size, the anchor symbol length will increase as log function of network size, since each sender is assigned a unique preamble and postamble as the local address. For example, a 2-byte anchor can address a maximum of 2^{11} senders each with a unique 16-bit preamble and postamble ($\frac{2^{16}}{2}$) and 4 initial bits for RF settling ($\frac{2^{15}}{2^4}$). The tradeoff between network scale and energy efficiency will determine the anchor symbol length in practice.

4.4.2 CSS Modulated Anchor Symbol. Although WiChronos achieves low probability of collisions through reduced time-on-air, as the network scale increases, the number of FSK-modulated anchor symbol length increases, negatively affecting the energy efficiency of the transmitter. The proposed CSS-modulated anchor symbols can accommodate more transmitters than FSK-modulated anchor symbol. In a network setting with C chirp symbols, the number of transmitters that can be accommodated using CSS increases exponentially as a function of C (Equation (8)). Additionally, due to it low false-positive, the minimum hamming distance between CSS-modulated anchor symbols can be lower than that of FSK, further reducing the anchor symbol duration. Therefore, CSS-modulated anchor symbols will lead to fewer collisions and hence can improve scalability. However, the step size of a chirp signal of CSS implementation using off-the-shelf radios are limited by the RF front end. In our design of eight chirps per anchor symbol (details in Section 6), the time to transmit one chirp is 38x the time to transmit one FSK symbol. The large time to transmit a chirp is due to the switching time of the oscillator. A dedicated CSS implementation of WiChronos will result in a lower probability of collisions.

5 ACCURACY-THROUGHPUT TRADEOFF

The promise of long battery life and range in a large-scale is achieved at the cost of data-rate. We achieve energy efficiency by offloading the communication burden to timers at the sender and the receiver and hence the data-rate of a link depends on the clock rate at the transceiver. Consider an

MCU with a clock rate $f_c = 32.768$ kHz. If increasing clock cycles each represent a value, a total of 32768 values can be conveyed in 1 s, i.e., 15 bits ($log_2(32768)$) can be communicated in one second (plus anchor symbol time). To generalize, the data-rate of a WiChronos link is given by

$$R_b = \frac{d \cdot f_c}{T_{info}}. \tag{11}$$

T_{info}, the time to transmit a d-bit message is in the range of $[0, 2^d - 1]$. For a uniformly distributed data source where the values of T_{info} are equiprobable, the expected value (average) of $T_{info} = 2^{d-1}$.

The achievable data-rate is lower than that of LPWAN technologies with comparable range. The numerator of data-rate in Equation (11) is a linear function of payload length while the denominator is an exponential function. This is in contrast with existing modulation techniques where the data-rate is a constant that is independent of the payload length. *WiChronos is thus not suitable for applications with high data-rate and low latency demands.*

5.1 Maximizing Data-Rate

We present two strategies to improve our data-rate performance: (1) Accurate higher clock rates and (2) Efficient Time encoding. As shown in Equation (11), the data-rate of WiChronos is directly proportional to the clock rate f_c at the transmitter. Increasing f_c reduces the time between the anchor symbols for the same number of clock cycles and improve data-rate. The accuracy of the clock plays a significant role in improving data-rate. Commercially available ultra low-power crystal oscillators [70], and MEMS clocks [71] offer high accuracy, high rate clocks. We will discuss the impact of clock skew on data-rate and accuracy later in the section.

The second strategy for improving data-rate is aimed at minimizing the average wait time between anchor symbols using a priori knowledge of the source distribution, analogous to source coding. The expected (average) time to transmit a d-bit message is

$$\mathbf{E} = \sum_{i=0}^{2^d-1} i \ \Pr(v(i)),$$

where $\Pr(v(i))$ is the probability of sensing a data value $v(i)$. Minimizing $\mathbf{E}$ will minimize the average time to send a value between 0 and $2^d - 1$, which will maximize the data-rate. This can be reduced to a continuous Knapsack problem [72], where the data values must be assigned a time value such that $\mathbf{E}$ is minimized. It has been proven that the optimum solution for continuous knapsack problem is achieved using greedy algorithm [72], i.e., arrange all possible sensor data in decreasing probability of occurrences and map to increasing time values in $[0, 2^d - 1]$. Mapping the most recurring data to the shortest time, we optimize the data-rate performance.

5.2 Timing Error Correction

The maximum achievable data-rate of a WiChronos link relies on the accuracy of clock rate, processing time, data transmission, and the propagation delay. Figure 7 presents a detailed timeline at a WiChronos transmitter. The currents and the duration listed are specific to the MCU and radio used in our prototype. By default, the radio and the MCU are in sleep mode. The total time to send data includes the radio wake-up time, the anchor symbol transmit time, and the information time. Timing errors in one or more of these components will affect the received T_{info}, leading to bit errors.

We broadly categorize bit errors in received data into the following categories, (1) errors in the anchor symbol, (2) anchor symbol loss, (3) processing and propagation time errors, and (4) clock counting error. Existing error detection and correction mechanisms are designed for bit errors and

require rethinking for timing errors. We propose a simple error detection mechanism for anchor symbol loss and correction mechanisms for bounded timing errors.

5.2.1 Anchor Symbol Error and Loss. Though we choose the receiver BW and anchor symbol length to minimize BER, there is a non-zero probability for anchor symbol error or loss. Existing coding techniques such as Hamming codes will be used to correct for single bit errors in the anchor symbol. Anchor symbol loss is detected using (1) timeout, (2) stateful receiver. We use the prior knowledge of the maximum payload length and the processing time at the sender to detect anchor loss using *timeout*. For each sender, the timeout value is set to $TO = t_{anchor} + T_{info-max}$, where t_{anchor} is the sum of maximum processing and transmission time to send an anchor symbol and $T_{info-max}$ is the maximum clock cycles mapped to a data. The receiver detects the loss of an anchor symbol whenever the counter exceeds TO. The second detection mechanism maintains the state of the anchor symbol reception for each sender. For every anchor symbol received, the receiver verifies the previous symbol received and the timer value is stored only if a postamble is followed by a preamble. Else, the counter value is discarded, reset, and marked as an error, since recurring postambles (or preambles) indicate loss of a preamble (or postamble).

5.2.2 Processing Timing Error. In Figure 7, let t_p be the average time to send an anchor symbol. t_p is composed of the time to perform the operations in MCU such as ADC, timer setup, serial communication, enter and exit sleep mode, radio wake-up time, modulation, and transmission. Variations in the number of cycles to execute any of these operations can vary t_p in the range $[-\epsilon, +\epsilon]$. We assume that the operations in the MCU are deterministic and do not contribute to ϵ. The radio wake-up time can vary within a bounded range ([28]). We correct for this timing error by triggering the data timer after $t_p + \epsilon$. On reading a sensor data of D, the MCU sets a *transmit counter* for $t_p + \epsilon$ cycles and triggers the radio module to transmit the preamble. At the end of the transmit counter, the MCU and the radio are set to sleep mode for D cycles. By increasing the transmit time from t_p to $t_p + \epsilon$, the transmitter removes the variability in the preamble (and postamble) transmit time. The receiver counts the number of cycles between the preamble and postamble and subtracts $(t_p + \epsilon)$ to obtain T_{info}. We correct for variations in t_p by increasing the overall time to transmit as, $t_{anchor} \geq t_p + \epsilon$. For timing errors bounded by ϵ, the increase in anchor symbol duration from t_p to $t_p + \epsilon$ can achieve 100% error correction.

5.2.3 Clock Cycle Error. Timing errors due to clock skew at the transceivers can lead to incorrect T_{info} and hence bit errors. We propose a simple error correction mechanism that spreads out the data value (in time) to account for the clock skew. Consider the 32 kHz crystal oscillator used in MSP430. Though the quartz crystal oscillators have high stability, it has a tolerance of ±30 ppm, resulting in an error of ±0.9 Hz in room temperature [70], i.e., the measured clock cycle can vary by ≈1 clock cycle. To correct for this clock counting error, we assign data value D to clock cycles that are separated by 3, i.e., the minimum difference between two adjacent T_{info} transmitted over air is set to three, to correct for variations in the clock cycles measured. To generalize, when using a clock rate with a tolerance of $\pm\delta$, the minimum difference between two transmitted clock cycles is set to δ. Therefore, a sensor data D is mapped to $\delta + D \cdot (2\delta + 1)$. Using the above redundancy in time to correct for clock cycle errors will reduce the effective data-rate since fewer unique clock cycles represent data. Therefore, accurate (low tolerance) clocks are crucial to the design of WiChronos. In addition to this, to check the accuracy of clocks, a pre-determined payload can be transmitted, but this is currently beyond the scope of our implementation and will be explored as a part of future work.

5.2.4 Propagation Error. The time to receive an anchor symbol includes the propagation delay of the RF signal. At distances of a few *kms*, propagation delays of RF signals traveling at the speed

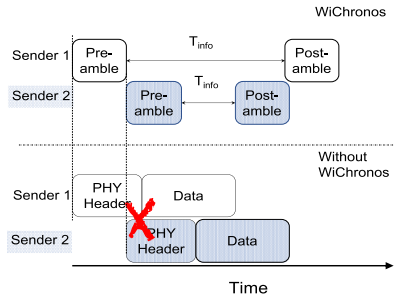

Fig. 8. Collisions in the network using ALOHA.

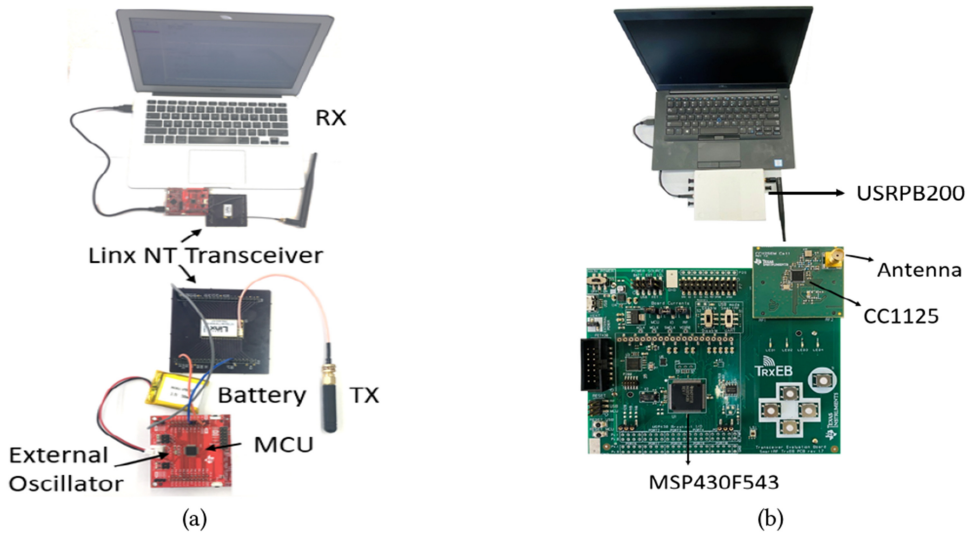

Fig. 9. WiChronos transmitter-receiver hardware: (a) FSK-modulation using Linx-NT as Tx and CC1125 as Rx (b) CSS-modulation using CC1125 as Tx and USRP B200 as Rx.

of light are on the order of μseconds. Therefore, changes in propagation delays would also be on the order few μseconds. Error correction mechanism proposed above for clock skew is modified to correct for propagation errors too. A 50% error in propagation delay at a distance of 10 km can lead to an error of ±0.8 cycles at a clock rate of 32 kHz. A priori estimate of channel and propagation model is used to encode redundancy. For bounded error in propagation delays, we can achieve 100% error correction by further increasing the minimum difference between adjacent T_{info}. Combining these error detection and correction mechanisms, WiChronos can correct for all bounded errors and detect symbol losses.

6 IMPLEMENTATION

WiChronos is implemented using off-the-shelf components such as general purpose radio modules as transmitters and software-defined-radio (USRP B200) as receivers, as shown in Figure 9. We implement the WiChronos transmitter by modulating the time between the start and stop anchor with the payload, as explained in Section 4. The transmitter uses a 32.678 kHz clock to encode data in the time interval between start and stop anchor. Since information is encoded in the time

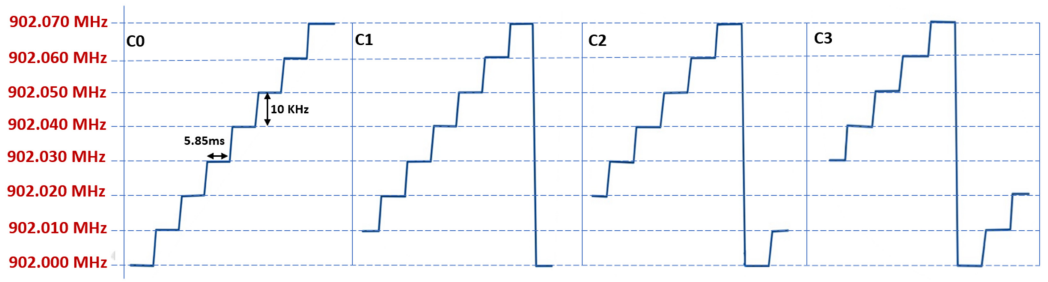

Fig. 10. Real USRP capture of four chirps generated using off-the-shelf radio modules with 10 kHz frequency step.

difference, absolute clock synchronization is not needed. The receiver counts $N_{samples}$, the number of samples received between the anchors. For a sampling rate of f_s samples/s at the receiver, we calculate the payload as

$$Payload = \frac{N_{samples} * 32678}{f_s}$$

In our implementation, we use a sampling rate of 140 kSamples/s on the USRP receiver. To correct bounded errors due to clock skew or the number of samples received, we implement the error correction mechanisms proposed in Section 5.2 at the receiver. We verify this error correction mechanisms experimentally and present our results in Section 7.6. In this work, we design and evaluate WiChronos using FSK-modulated anchor symbols as well as CSS-modulated anchor symbols, operating in the 902–928 MHz ISM band. The anchor symbol design derived for each of the modulations in Section 4.2 is implemented using the off-the-shelf components, as described below.

FSK-Modulated Anchor Symbol. We use Linx-NT radio module along with TI MSP430FR2355, an ultra-low power microcontroller to implement NB (100 to 200 kHz) FSK-modulated anchor symbols. NB anchor symbols are transmitted at a baud rate of 9.6 kbps. Linx-NT was chosen for its ease of programming, as it allowed hardware control to choose parameters such as the center frequency, BW, and baud rate. UART interface was used to send and receive anchor symbols to the radio. We implement ultra-NB (10 to 100 kHz) FSK using TI CC1125 as the radio module. Ultra-NB anchor symbols are transmitted at a baud rate of 1.2 kbps. We test the energy, range, and the collision performance at different BWs, varying from 10 kHz to 200 kHz. We also tabulate the packet error rate at different SNRs that correspond to different distances. We use 3-dB gain, quarter-wave whip antennas. WiChronos receiver for FSK-anchor symbols is implemented using TI CC1125 evaluation board.

CSS-Modulated Anchor Symbol. We utilize CC1125 to design and implement a novel chirp generation code. By default CC1125 allows us to choose a modulation from FSK, OOK, and MSK and does not offer CSS. However, it has a feature to transmit an unmodulated carrier signal at a given frequency. We use this feature to implement CSS. At the rise of each clock cycle, the center frequency of the unmodulated carrier is increased by f_{step}, as illustrated in Figure 10. This is repeated until the entire BW is covered. To generate chirps with a desired initial frequency, we start with the corresponding frequency, linearly increase to BW and continue to increase, as illustrated in Figure 10. As designed in Section 4.2, the preamble of a CSS-modulation anchor symbol is a sequence of four up-chirps (C0) (Figure 5). The chirps are generated in the 902–928 MHz frequency range over a BW of 70 kHz. Due to the limitations of the CC1125 hardware, the minimum step size in frequency that can be detected and demodulated accurately is 10 kHz. We implement

(a) (b)

Fig. 11. WiChronos experimental setup in outdoor deployments: (a) NB FSK-modulation (b) Ultra NB FSK-modulation and CSS.

a chirp by increasing the frequency of transmission by 10 kHz on each clock cycle. The fastest clock rate achievable by the CC1125 hardware to successfully increase the frequency by 10 kHz at each rising clock edge is 170 Hz. Each chirp has eight steps and occupies a BW of 70 kHz, thus making it a NB signal. Since one of these chirps is the preamble, seven unique chirps allow 2,401 unique combinations. Therefore, eight chirps can accommodate a network of 1,200 nodes.

CSS demodulation, inspired by LoRa demodulation, is implemented on USRP B200 receiver using GNURadio. The complex I/Q samples received at the USRP are multiplied with a down chirp to detect the preamble. On detecting the presence of a preamble, we perform coarse and fine grained chirp synchronization, similar to LoRa demodulator [73], to accurately detect the start of the packet. We then proceed to demodulate the anchor symbols following the same process of multiplication with a down chirp followed by FFT.

7 EVALUATION

7.1 Experimental Setup

We evaluate WiChronos using FSK and CSS-modulated anchor symbols in both indoor and outdoor setting. The outdoor experiment was performed at distances upto 4 km between the transmitter and the receiver in urban locations, as shown in Figure 11. The indoor, controlled experiments are performed in an office space of 15 m × 10 m. As shown in Figure 9, the transmitter is powered by a battery and the receiver is always on and connected to a laptop. For all our experiments (FSK and CSS), we have connected ZHL-42W power amplifier to our receiver to amplify incoming signals. The power amplifier provided a gain of about 25 dB in addition to the 2 dB gain from the antenna. Our implementation, circuit design, and hardware setup to recreate our results is publicly available.[1]

We compare the energy efficiency, communication range, and theoretical collision performance of WiChronos against LoRa experimentally and present analytical comparison with SigFox. Easy-to-program, Arduino-based LoRa module [74] (RFM69HCW) does not allow for energy management and has low battery life. We implemented an energy management module in SX 1272 [75] operated using MSP430 for fair comparison; we reduce its preamble to 6 bytes, remove Cyclic Redundancy Check and MAC headers, disable ACKs, and set to transmit-only mode to minimize its energy consumption and provide fair comparison. Throughout this section, unless otherwise

[1] https://github.com/Yaman-Sangar/WiChronos.

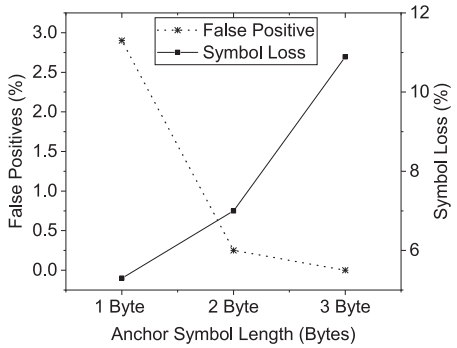

Fig. 12. Experimental verification of FSK-modulated anchor symbol length.

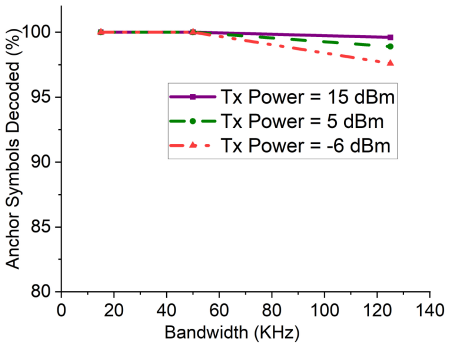

Fig. 13. FSK-modulated anchor symbols decoded as a function of receive BW.

mentioned, we operate LoRa and Linx at 915.37 MHz center frequency and CC1125 at 905 MHz center frequency. LoRa is implemented at an SF of 7, coding rate 4/5, and BW of 125 kHz.

Toward the evaluation of WiChronos, we perform experiments to evaluate the following:

—*Efficiency of anchor symbol design:* What is the false positive rate of anchor symbol reception? What is the accuracy of anchor symbol demodulation?
—*Energy-efficiency:* What is the battery life of WiChronos compared to state-of-the-art? What is the impact of network scale on energy efficiency?
—*Communication Range:* What is the achievable communication range of WiChronos with the two anchor symbol designs proposed? How is range affected by BW and modulation?
—*Network Scalability/Medium Access Control:* How many transmitters can WiChronos accommodate with a low probability of anchor symbol collisions? What is the overall network throughput?
—*Data-rate:* What is the achievable data-rate per-node and its efficacy to correct bounded timing errors?

7.2 Anchor Symbol Design

In this section, we evaluate the NB-FSK, ultra-NB FSK, and CSS-modulated anchor symbol designs presented in Section 4.2. We design the length to achieve an SNR $\geq$ 10 dB resulting in a BER of 10^{-3} for BFSK [58]. At BER = 10^{-3}, we determine the optimum symbol length to be 10 bits, with a false positive probability $P_f \leq 0.01$ and symbol error probability $P_e \leq 0.001$ from Figure 3. Linx allows integer multiples of bytes (not bits) and hence we choose a 2-byte anchor symbol. For FSK-modulated anchor symbol, we implement the first byte to be a sequence of alternating 1s and 0s to indicate the start of message and the second byte to be an 8-bit address uniquely assigned to a transmitter.

In Figure 12, we experimentally determine P_f and P_e for varying NB FSK-anchor symbol lengths. With increasing length, P_f decreases while P_e increases. At 2-byte anchor symbol, P_f is below 0.01 and P_e below 0.08. The experimental P_e is higher than the expected P_e derived in Equation (7) due to intermittent pedestrian traffic and strong winds. We present the impact of other environmental conditions on the symbol error rate later in the section.

Next, we study the impact of receiver BW on decodability. In Figure 13, we plot the percentage of FSK-modulated anchor symbols decoded correctly as a function of receive BWs, for different transmit powers. For a given transmit power, as BW increases, the noise floor increases and hence SNR decreases, resulting in fewer anchor symbols decoded. At BW = 15 kHz, 100% of the symbols

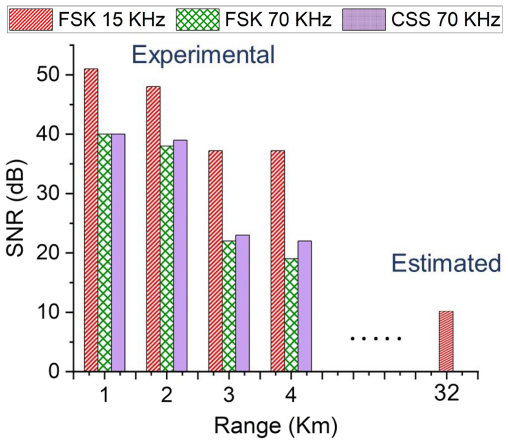

Fig. 14. Experimental WiChronos SNR at increasing ranges till 4 km and estimated SNR at 32 km.

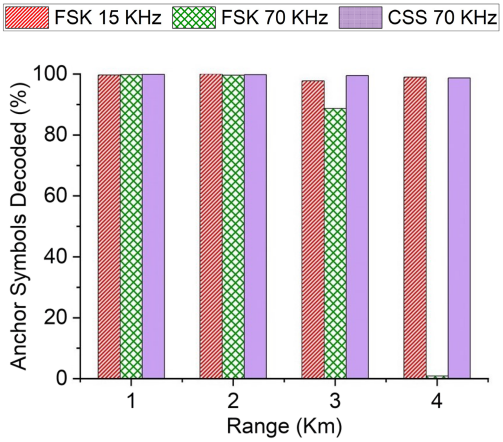

Fig. 15. Anchor symbols decoded at increasing distances as a function of modulation and BW.

are decoded correctly at all transmit powers. At BW= 120 kHz however, this decreases to about 98%. Hence, operating in ultra-narrow bandwidth improves SNR and, in turn, decodability.

We also compare the performance of FSK- and CSS-modulated anchor symbols. In Figure 14, we plot the SNR of the anchor symbols at the receiver for varying BWs (15 and 70 kHz) and anchor symbol modulation (FSK and CSS). It can be noticed that the SNR of 15 kHz is higher than that of 70 kHz, irrespective of the modulation. This is due to the dependence of SNR on the receive BW. However, the number of anchor symbols decoded also depends on the modulation. Despite the use of same 70 kHz BW and comparable SNR, since CSS is inherently resilient to channel noise and interference, it outperforms NB FSK, as shown in Figure 15. Hence, NB offers an improvement in SNR while CSS offers more error resilience for the same BW, due to its processing gain.

From experiments, we infer that the Linx-NT has a higher than average carrier sensing time, resulting in higher false positives. RF modules with smarter carrier sensing can further reduce P_f and hence the anchor symbol length. In addition to that, the maximum transmit power of Linx-NT and CC1125 is 13.5 dBm and 15 dBm, respectively, while FCC allows up to 30 dBm, which will improve the accuracy of anchor symbol demodulation. The presented result is thus an upper bound on the anchor symbol length and offers room for a further decrease in symbol length. When CSS modulation is used for anchor symbols, the resilience to channel noise increases the accuracy of the received symbols. *In the rest of our evaluation, we use 2-byte anchor symbols for FSK and 8 chirp symbols for CSS, unless stated otherwise.*

7.3 Long Range

We evaluate the range performance of WiChronos experimentally as well as analytically in this section. The long-range performance of WiChronos depends on the radio module and the modulation parameters used for anchor symbol. The impact of BW on anchor symbols decoded was presented in Figure 13. We experimentally evaluate the maximum achievable range in outdoor experiments in urban streets (Figure 11) with traffic.

In Figure 14, we plot the experimentally received SNR at increasing distances for the three anchor symbol modulations proposed. As expected, ultra NB FSK (15 kHz BW) has the highest SNR due to its low noise floor. As attenuation of signal power increases with increase in the distance, we expect a drop in SNR at higher distances, affecting decodability. As expected, the SNR of 70 KHz FSK and CSS are comparable, since SNR is a function of the receive BW. This is because

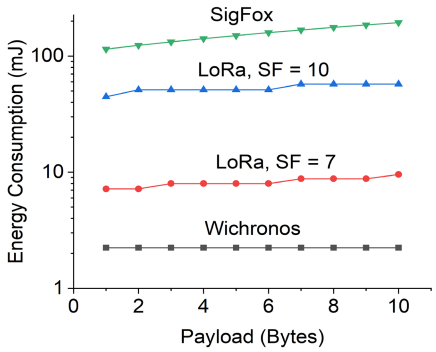

Fig. 16. Energy Consumption of WiChronos vs LoRa and SigFox.

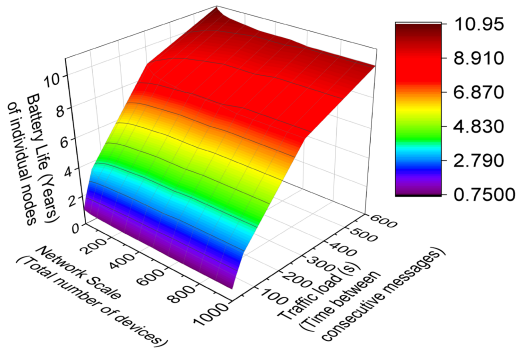

Fig. 17. Battery life of WiChronos vs scale and traffic load.

the noise floor is a function of BW and is unaffected by the modulation. Despite this, CSS achieves higher packet decodability due to the spread spectrum gain as shown in Figure 15. In other words, CSS enables the receiver to decode anchor symbols even when buried under noise, thus improving the communication range. Using our outdoor experimental setup, we verify that at distances up to 2 km, all the modulations achieve close to 100% packet decodability. This however drops quickly for 70 kHz FSK as the SNR drops below 20 dB over 3 km. CSS, on the other hand, continues to decode over 99% of the anchor symbols at 4 km. Similarly, ultra-NB FSK decodes over 99% of the anchor symbols at 4 km.

We extrapolate the SNR from the above experiment to estimate the maximum achievable range of ultra NB FSK-modulated to be 32 km. From the free space path loss equation, 6 dB loss is expected when the distance doubles. However, in our experimental evaluation, we found that SNR drops by 9 dB for every doubling in distance. We use this 9 dB loss and estimate that at ranges of 32 km between the transmitter and the receiver, the received SNR is greater than 10 dB and hence can be reliably decoded.

In conclusion, the achievable range of our prototype is constrained by the hardware, BW, and modulation and is not an inherent limitation of WiChronos. Any RF module with a protocol-free mode can be integrated with an MCU to implement WiChronos. SNR at the receiver can be further improved by increasing the transmit power. RF modules with the maximum allowable **Effective Isotropic Radiated Power** (**EIRP**) and ultra-NB FSK or CSS modulated anchor symbols can reach distances of over 30 km.

7.4 Energy Efficiency

A key contribution of WiChronos is the improved battery life due to reduced time-on-air. We evaluate the energy consumption of WiChronos with 2-byte anchor symbol and compare with LoRa and SigFox. We design a power management block that powers down the radio completely when it is not actively transmitting. We only consider the power consumption of the radio module and the micro-controller power is ignored for all the technologies for fairness.

In Figure 16, we compare the energy consumption for varying payload lengths. The energy consumption of WiChronos is approximately 2.03 mJ, the lowest among the three technologies. Our energy consumption remains the same for any payload length, as energy is only a function of the anchor symbol length.

When transmitting a 2-byte payload, WiChronos reduces energy consumption by **3x** compared to LoRa-SF7, **23x** to LoRa-SF10, and **55x** to SigFox (BW normalized). The reduced energy consumption of WiChronos, which increases with payload length, is due to, (1) reduced air-time

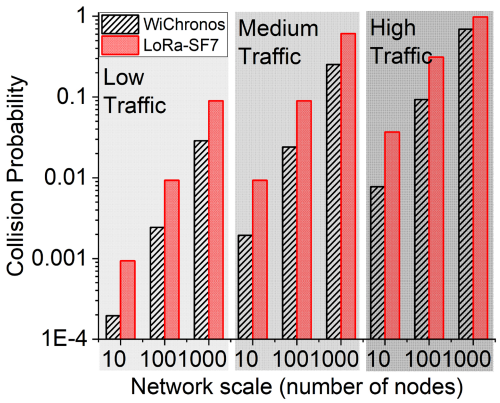

Fig. 18. Collision performance in a network of FSK anchor based WiChronos and LoRa SF-7.

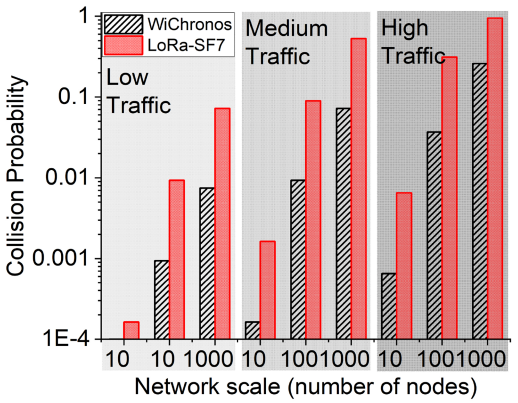

Fig. 19. Collision performance in a network of CSS anchor based WiChronos and LoRa SF-7.

and (2) non-increasing energy-per-bit E_b. E_b for a WiChronos sender decreases with increasing payload as the overall energy remains constant while the number of bits increases. In classical modulation, E_b is constant and hence their energy increases with payload length. The energy efficiency will be further improved by using modules with smaller sleep currents and faster wake-up time.

The energy efficiency of WiChronos depends only on the length of the anchor symbol and the traffic load. Figure 17 shows the impact of traffic load and network scale on the battery life of a single node. For a given traffic load, battery life of a node decreases with increasing network scale, since the anchor symbol length increases with scale. At higher traffic loads where a payload is being sent once every 15 or 30 seconds, the battery life reduces considerably as compared to low traffic scenarios. As discussed earlier, WiChronos derives energy savings partly from reducing the time-on-air which increases significantly when the traffic load and/or the scale increases.

7.5 Multiple Access Control

In this section, we analytically and experimentally evaluate the throughput performance of WiChronos network using ALOHA as the MAC protocol.

7.5.1 Collision Performance. We present the probability of collisions in y-axis as a function of network scale under varying traffic conditions in Figure 18 for WiChronos with NB FSK based anchor symbol. The background grey shade darkens as the traffic load increases. We categorize the traffic load as high, medium, and low when a 2-byte payload is sent every 15 s, 60 s, and 600 s, respectively.

As shown in Figure 18, the estimated probability of collision for WiChronos in a 100-node network with high traffic is **3.4x** and **10.4x** higher compared to LoRa with SF-7 and SF-10, respectively. At low traffic, it is **3.8x** and **30x** higher compared to LoRa-SF7 and SF-10, respectively. To compare against SigFox, we use a BW of 600 Hz for both WiChronos and SigFox. For low traffic, collision probability for WiChronos is **37.6x** compared to SigFox.

In Figure 19, we present the probability of collisions using CSS modulated anchor symbol. The collision probability in a 100-node network with high traffic for WiChronos is **8.6x** and **27.1x** higher compared to LoRa with SF-7 and SF-10, respectively. At low traffic, the collision probability for WiChronos is **10.3x** and **98.8x** higher compared to LoRa with SF-7 and SF-10, respectively. Under low traffic conditions, the collision probability for WiChronos is **68.5x** higher than SigFox. The

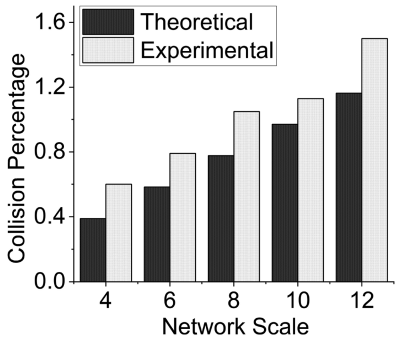

Fig. 20. Experimental vs Theoretical comparison of collision probability.

collision probability of WiChronos implemented with CSS based anchor symbol is lower than the FSK based implementation across all scales and traffic loads. For a network of 100 nodes, the collision probability of CSS based implementation of WiChronos is 2.5x lower than that of FSK based implementation in all traffic scenarios. This reduction is due to lower anchor symbol duration.

Note that the collision probability increases with both network scale and traffic, due to larger volume of data, resulting in higher vulnerability to collisions. This increase in collisions is lower for WiChronos than that of LoRa and SigFox due to its reduced time-on-air. Since the channel is active only for the duration of the anchor symbols, the vulnerable period for collision of WiChronos is smaller for the same BW and payload length.

We also validate the theoretical results with experiments for high-traffic, small-scale network (zoomed-in image) on WiChronos implemented with NB FSK based anchor symbols in Figure 18 in a network of 12 senders in heavy traffic scenario. We program the senders to wake up every 16 seconds to communicate a random 2-byte payload. The senders are randomly placed inside a 15 m $\times$ 10 m office space. The experimental results reflect the cumulative losses due to collisions, false positives, and anchor symbol losses. On an average, the theoretical collision rate is 75% of the experimental rate; the theoretical results are an approximation for a large-scale network and we expect the experimental results to match theoretical for larger networks.

7.5.2 Network Goodput Performance. The reduced collision also improves the average network goodput performance (total number of successful data bits in the network in a given duration). We present the average network goodput as a function of traffic load for various network scales in Figures 21–24, where each transmitter sends a 2-byte message every *traffic-load* seconds. The above results are BW normalized for fairness, with WiChronos and LoRa using 100 kHz and 125 kHz, respectively, in Figures 22 and 24 and 600 Hz for WiChronos and SigFox in Figures 21 and 23. In Figures 23 and 24, we plot the goodput of WiChronos implemented with CSS based anchor symbol against LoRa and SigFox, respectively.

Due to an increase in the volume of data, the goodput increases with traffic initially. However, it reaches a maximum value, beyond which collisions dominate and reduce the number of successful transmissions, in turn, reducing goodput. For a given scale, the goodput of WiChronos outperforms LoRa due to its reduced collisions (Figure 18), and they converge at lower traffic. This is because, with reduced traffic load, data volume is low, inversely affecting goodput due to lower utilization of channel capacity. We compare the goodput performance of WiChronos and SigFox in Figures 21 and 23. As the scale increases, the increase in collision probability of SigFox is higher than that of WiChronos. Similarly, with reduced traffic load, the decrease in collision is higher for WiChronos, leading to a better goodput.

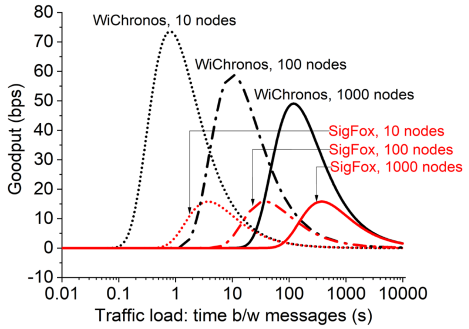

Fig. 21. Network goodput of WiChronos with FSK modulated anchor and SigFox as a function of traffic load.

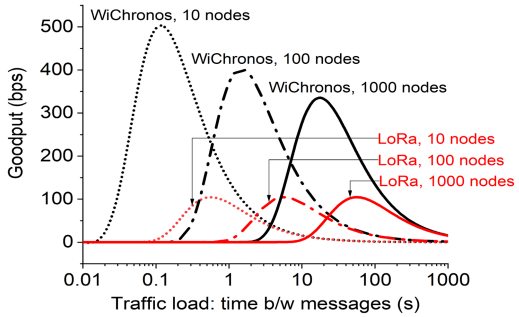

Fig. 22. Network goodput of WiChronos with FSK modulated anchor and LoRa SF-7 as a function of traffic load.

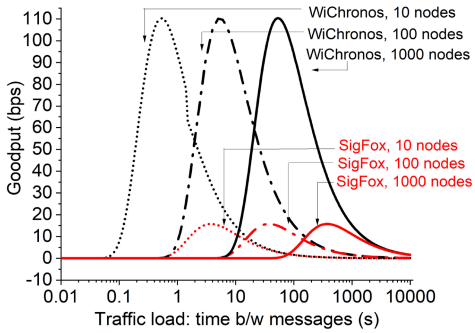

Fig. 23. Network goodput of WiChronos with CSS modulated anchor and SigFox as a function of traffic load.

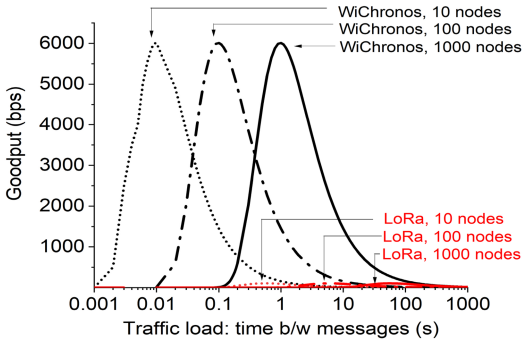

Fig. 24. Network goodput of WiChronos with CSS modulated anchor and LoRa SF-7 as a function of traffic load.

It must be noted that though WiChronos outperforms LoRa and SigFox in average network goodput, it trades off instantaneous goodput. In a 1000-node network where each node has a 2-byte payload every 10 minutes, the instantaneous goodput of a WiChronos and a LoRa node are 15.0 bps and 517.27 bps, respectively. Similarly, with 600 Hz BW, the instantaneous goodput of WiChronos and SigFox are 12.08 bps and 46 bps, respectively. WiChronos is therefore best suited for applications with short payloads, where it can deliver low-energy over long-range in a large-scale.

LoRa can leverage the orthogonality of SF to enhance scalability [76]. Lower SF values offer high data rate, and low energy. High SF values help attain a greater range at the cost of data-rate. While using different SF could help with scalability, it will also effect the range and battery performance. Another option offered by LoRa and SigFox is to use **Frequency Division Multiple Access (FDMA)**. FDMA can be used in addition to ALOHA to further reduce the collision rate of WiChronos as well. For a given receiver BW, the reduced BW on each sender will increase the collision rate. However, this is only a function of the anchor symbols for WiChronos and the effect will be less pronounced compared to LoRa and SigFox. The decrease in collision rate from the reduced number of devices per channel outweighs the increase (Figure 19) due to lower BW.

7.6 Error Correction and Data-Rate

We identified four categories of error viz., anchor symbol loss, processing time error, clock skew error, and propagation error. The results presented in the rest of this section incorporate the

Table 3. Impact of Clock Rate and Skew on Data-Rate

Clock Rate	Tolerance ppm	Tolerance cycles	Expt. Tolerance cycles
1 MHz [59]	±10000	±10000	±720
32.678 kHz [70]	±30	±1	±1
1 MHz [71]	±50	±5	Not validated

anchor symbol loss detection. For the other three errors, we evaluate the data-rate performance of WiChronos, the accuracy of received data in the presence of timing error, and the impact of the proposed error correction mechanisms on data-rate. We implement the error correction mechanisms proposed in Section 5.2 at the transceivers.

7.6.1 Processing Time Error Correction. Figure 7 shows the timeline of WiChronos data transmission, where the duration and currents are specific to the components used in our implementation. As discussed in Section 5.2, processing time error is corrected by elongating the transmission time t_p to $t_p + \epsilon$. For the system under consideration, $t_p = 196$ cycles and the estimated $t_p + \epsilon = 276$ cycles. At system clock rate of 32.678 kHz, the components of t_p with their corresponding average (A) and maximum (M) clock cycles are (1) Radio wake-up time + MCU processing (A:137, M:200), (2) MCU processing (A:8, M:8), and (3) 2-byte anchor symbol transmission time at 9.6 kBaud (A:51, M:68). We estimate the upper bound of each operation to determine ϵ, and validated experimentally. On reading a sensor data, the MCU sets *TimerB* to count up to 276 cycles during radio wake-up and anchor transmission. The effective processing and transmission time is therefore a predetermined constant (276 cycles) and variations within this upper bound does not affect the measured T_{info} at the receiver. The receiver counts T_{info} and subtracts 276 to decode data, achieving 100% accuracy.

7.6.2 Clock Skew Error. Clock skew directly affects the accuracy of the data received. We evaluate the performance of the two clocks present in MSP430 (1) an **external crystal oscillator** (**ECO**) and (2) an internal **Digitally Controlled Oscillator** (**DCO**) and analyse their impact on data-rate. Columns 2–4 in Table 3 show the clock rate and worst case tolerance of these clocks, along with other commercially available low-power clocks. Clock tolerance is an indicator of the accuracy of the clock. For example, with the 32.678 kHz ECO with a tolerance ±30 parts per million [70] the measured number of clock cycles vary only by ±1 cycle. We experimentally verified the tolerance levels of the ECO and the DCO by transmitting a predefined value of T_{info} every minute for over a week. Column 5 shows the tolerance determined experimentally for the ECO and DCO. Note that the theoretical tolerance values are an upper bound. Therefore, the clock skew correction proposed in Section 5.2 uses the tolerance values to determine δ. For the ECO, since $\delta = 1$, a data D is mapped to $T_{info} = 3D + 1$. We correct for clock skew by introducing redundancy, which reduces the effective number of data values D that can be communicated, reducing the data-rate.

Higher tolerance requires higher redundancy for correction, negatively affecting data-rate. Figure 25 plots the achievable data-rate as a function of payload for different clocks. When using clock skew error correction, the tolerance has a higher impact on the data-rate than the clock frequency. For a given tolerance, the data-rate of WiChronos with 32 kHz and 1MHz are comparable, due to the redundancy introduced for clock skew correction. Accurate clocks are key to the success of WiChronos. Low-power, high accuracy clocks in the order of MHz [71] can be integrated with the MCU to improve the data-rate performance of WiChronos. Note that the data-rate decreases with increasing payload length, irrespective of clock tolerance, due to the exponential dependence of information time on the payload. Prior knowledge of source distribution can help with optimum data-time encoding to improve data-rate.

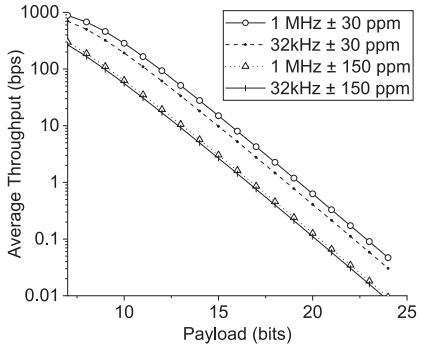

Fig. 25. Datarate performance.

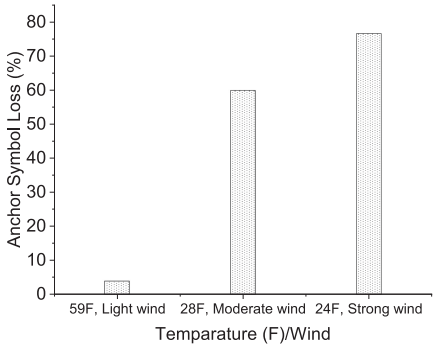

Fig. 26. Impact of environmental conditions.

7.7 Environmental Conditions

We evaluated WiChronos outdoors under varying weather and traffic conditions. Figure 26 shows the impact of temperature and wind on the anchor symbol error rate at a distance of 250 m. SER increases by a factor of 15 at low temperatures and 19 when there are strong winds as well. While this is not a complete analysis, it indicates the strong impact of environmental conditions on anchor symbol loss, and, in turn, bit errors at the receiver. We plan to explore the impact of environmental conditions and design antennas and protective casing to reduce the impact in our future work.

8 RELATED WORK

Timing interval based communication has been studied in the past. We present an overview of these works below.

Information Theoretic Analysis: An information theoretic analysis of encoding information in the queuing time has been studied in literature [77–81]. While bounds on channel capacity of single-queue and multiple-queue servers worst-case timing error distributions have been studied, they do not provide algorithms for energy efficiency and/or long-range communication in a wireless system. The maximum achievable data-rate of WiChronos aligns with the capacity of timing channel derived in [77].

Timing Channel: Timing based communication has been studied as a security risk in covert timing channels [82–84], where information is encoded covertly in the time interval. The majority of the research work on timing channels has focused on defense mechanisms to eliminate timing channels.

Pulse Time Modulation: This work is motivated by **Pulse Position Modulation** (**PPM**) and Communication through Silence [85], a challenges paper on timing based modulation in WSN. Reference [85] does not consider long-range and scalability in wireless networks. It does not consider the challenges in the practical implementation of timing interval modulation in wireless networks such as anchor symbol length, synchronization, and packet errors. To the best of our knowledge, WiChronos is the first attempt at implementing timing interval modulation technique for long-range, energy efficient communication in wireless networks.

PPM and its variants such as Differential PPM [86, 87], M-ary PPM [88–92] have been developed and widely used in one-to-one optical networks with ultra wide BW and narrow pulses. The following requirements of typical PPM implementations make them challenging for wireless networks.

Bandwidth requirements: PPM and its variants typically use an ultra-wide BW [88] to get a narrow pulse to achieve reasonable data-rates while also saving energy. Ultra wide band will result

in an increase in energy consumption and noise floor in a wireless module, affecting both battery life and range. To overcome this challenge, we use NB and achieve long range.

Clock Synchronization: In UWB, the pulses are short and therefore symbol synchronization is required for PPM. DPPM, however, overcomes this challenge by encoding in the time difference between pulses [86]. In this work, we relax synchronization requirements with the help of differential modulation and low data-rates. PPM implemented in one-to-one optical links does not require a dedicated MAC protocol. However, in a wireless network, the pulses collide on air and therefore dedicated addressing and MAC protocol is required [93–96]. Multiple transmitters, therefore, cannot share the channel without incurring packet losses or increasing energy consumption [97, 98]. In this work, we remove the need for MAC by uniquely identifying the transmitter in each pulse.

Despite its energy efficiency, PPM is not popular in wireless owing to the above challenges. We propose WiChronos, a special case of the more general PPM for wireless communication and design the modulation to cover a long range and accommodate a large scale.

9 LIMITATIONS AND FUTURE WORK

In this section, we discuss in detail the limitations and open research challenges that need further investigation as well as research areas stemming from our work.

Timing error detection and correction: Existing error correction codes are designed for bit errors. Timing errors in WiChronos can occur due to distance, clock errors, and channel conditions. Currently, we transmit anchor symbol at low data-rates of the order of few kbps, and hence the impact of above conditions on anchor symbol timing is minimal. Error correction mechanisms will be needed for higher anchor symbol rates of 100s of kbps. We proposed a simple error correction mechanism for clock skew that uses the a priori knowledge of the clock tolerance. Smarter, capacity achieving timing error correction is needed to improve the data-rate performance of WiChronos.

Impact of environmental conditions on clock rate and clock aging: We observed that at temperatures below 30°F (0°C), moderate to strong winds significantly affected the anchor symbol decodability. While it can be partly attributed to antenna stability, further experimental study on the impact of environmental conditions on packet decodability and clock accuracy is required.

Payload Length: When size of the payload increases, time required to wait for transmission of data increases, decreasing data-rate and throughput per node. Therefore, WiChronos is not suitable for applications requiring larger payloads. In order to use WiChronos for higher payload applications, an optimal way of encoding data to clock cycles is required. This implementation is currently beyond the scope of this project and can be part of future work.

Data-rate energy tradeoff: WiChronos trades off data-rate for energy efficiency. This is especially the case when data required to be transmitted increases, leading to increase in time to send data, reducing throughput per node. We propose two strategies to improve the data-rate performance of WiChronos. (1) A greedy algorithm that uses prior knowledge of the source distribution. (2) Information-theoretic and machine learning approaches to learn the source distribution and encode data to clock cycles optimally. Systems research on efficient low-power, high accuracy clocks have the potential to maximize data-rate and minimize energy further.

Anchor symbol loss: We use timeout to detect anchor loss when messages are shorter than the sensing period. However, when the time between messages decreases, anchor symbol loss can go undetected, leading to inaccurate reception. Further research to handle multiple anchor losses is required to broaden our impact.

Information security and authentication: In its current design, a WiChronos receiver identifies the sender from the anchor symbols and does not offer a mechanism for authentication. An adversary could be listening to the channel to decode data and it is therefore not secure. Encrypting anchor symbol bit pattern can be used to authenticate the sender whereas data security can

be achieved by encrypting the data (D) to timing (T_{info})mapping. Simple and efficient security protocols for timing-based communication is a branch of research that is open for further study.

Medium Access Control: A hybrid of FDMA- or CDMA-based ALOHA can potentially improve the reliability of WiChronos within the energy budget. MAC algorithms leveraging spatial diversity and anchor symbol modulation is a future extension of this work.

10 CONCLUSIONS

We propose WiChronos, a modulation technique that enables long-range communication in large-scale deployments of energy-constrained sensor nodes. By offloading the communication complexity to timers present in every MCU, we reduce the energy consumption and the cost of each sender. We reduce the time-on-air by minimizing the number of symbols per message, in turn, improving the spectral efficiency. The reduced time-on-air enables an ALOHA-based MAC protocol to accommodate a large-scale network without significantly affecting the collision performance. We propose error detection and correction mechanisms for timing induced bit errors for bounded errors. We prototype WiChronos using a variety of off-the-shelf, general-purpose RF modules, MCUs, and modulation techniques to evaluate the energy, range, and scale performance experimentally in indoor and outdoor scenarios.

REFERENCES

[1] Mare Srbinovska, Cvetan Gavrovski, Vladimir Dimcev, Aleksandra Krkoleva, and Vesna Borozan. 2015. Environmental parameters monitoring in precision agriculture using wireless sensor networks. *Journal of Cleaner Production* 88 (2015), 297–307.

[2] J. A. López Riquelme, Fulgencio Soto, J. Suardíaz, P. Sánchez, Andres Iborra, and J. A. Vera. 2009. Wireless sensor networks for precision horticulture in Southern Spain. *Computers and Electronics in Agriculture* 68, 1 (2009), 25–35.

[3] Hanwook Chung, Jingjie Li, Younghyun Kim, and Christopher Y. Choi. 2018. Continuous and wireless skin contact and ear implant temperature measurements and relations to the core body temperature of heat stressed dairy cows. In *Proceedings of the 10th International Livestock Environment Symposium*. American Society of Agricultural and Biological Engineers, 1.

[4] Haider Jawad, Rosdiadee Nordin, Sadik Gharghan, Aqeel Jawad, and Mahamod Ismail. 2017. Energy-efficient wireless sensor networks for precision agriculture: A review. *Sensors* 17, 8 (2017), 1781.

[5] National Soil Moisture Network. ([n. d.]). Retrieved from http://nationalsoilmoisture.com/.

[6] National Ecological Observatory Network. ([n. d.]). Retrieved from https://www.neonscience.org/.

[7] Decagon 10HS Soil Moisture Sensor. ([n. d.]). Retrieved from http://www.labcell.com/environmental/soil-moisture-sensors/10hs-soil-moisture-sensor.

[8] EC5 Soil Moisture Sensor. ([n. d.]). Retrieved from http://www.labcell.com/environmental/soil-moisture-sensors/ec5-soil-moisture-sensor.

[9] TEROS 12: Avanced soil moisture sensing. ([n. d.]). Retrieved from https://www.metergroup.com/environment/products/teros-12/.

[10] Deepak Ganesan Pan Hu, Pengyu Zhang. 2015. Laissez-faire: Fully asymmetric backscatter communication. In *Proceedings of the 2015 ACM Conference on Special Interest Group on Data Communication*. ACM, 255–267.

[11] V. Pillai, H. Heinrich, D. Dieska, P. V. Nikitin, R. Martinez, and K. V. S. Rao. 2007. An ultra-low-power long range battery/passive RFID tag for UHF and microwave bands with a current consumption of 700 nA at 1.5 V. *IEEE Transactions on Circuits and Systems I: Regular Papers* 54, 7 (2007), 1500–1512.

[12] Vincent Liu, Aaron Parks, Vamsi Talla, Shyamnath Gollakota, David Wetherall, and Joshua R. Smith. 2013. Ambient backscatter: Wireless communication out of thin air. *ACM SIGCOMM Computer Communication Review* 43, 4 (2013) , 39–50.

[13] Vamsi Talla, Mehrdad Hessar, Bryce Kellogg, Ali Najafi, Joshua R. Smith, and Shyamnath Gollakota. 2017. Lora backscatter: Enabling the vision of ubiquitous connectivity. *Proceedings of the ACM on Interactive, Mobile, Wearable and Ubiquitous Technologies* 1, 3 (2017), 105.

[14] Yao Peng, Longfei Shangguan, Yue Hu, Yujie Qian, Xianshang Lin, Xiaojiang Chen, Dingyi Fang, and Kyle Jamieson. 2018. PLoRa: A passive long-range data network from ambient LoRa transmissions. In *Proceedings of the 2018 Conference of the ACM Special Interest Group on Data Communication*. ACM.

[15] Shahin Farahani. 2011. *ZigBee Wireless Networks and Transceivers*. Newnes.

[16] Carles Gomez, Joaquim Oller, and Josep Paradells. 2012. Overview and evaluation of bluetooth low energy: An emerging low-power wireless technology. *Sensors* 12, 9 (2012), 11734–11753.
[17] Colby Boyer and Sumit Roy. 2014. —Invited paper—backscatter communication and RFID: Coding, energy, and MIMO analysis. *IEEE Transactions on Communications* 62, 3 (2014), 770–785.
[18] Thomas M. Cover and Joy A. Thomas. 2012. *Elements of Information Theory*. John Wiley & Sons.
[19] LoRa. ([n. d.]). Retrieved from https://www.semtech.com/lora.
[20] SigFox. ([n. d.]). Retrieved from https://www.sigfox.com/en/sigfox-iot-radio-technology.
[21] NB-IoT. ([n. d.]). Retrieved from https://www.gsma.com/iot/narrow-band-internet-of-things-nb-iot/.
[22] Juha Petäjäjärvi, Konstantin Mikhaylov, Matti Hämäläinen, and Jari Iinatti. 2016. Evaluation of LoRa LPWAN technology for remote health and wellbeing monitoring. In *Proceedings of the 2016 10th International Symposium on Medical Information and Communication Technology*. IEEE, 1–5.
[23] Ruslan Kirichek and Vyacheslav Kulik. 2016. Long-range data transmission on flying ubiquitous sensor networks by using LPWAN protocols. In *Proceedings of the International Conference on Distributed Computer and Communication Networks*. Springer.
[24] Amalinda Gamage, Jansen Christian Liando, Chaojie Gu, Rui Tan, and Mo Li. 2020. *LMAC: Efficient Carrier-Sense Multiple Access for LoRa*. ACM, New York, NY. DOI: https://doi.org/10.1145/3372224.3419200
[25] Khaled Q. Abdelfadeel, Dimitrios Zorbas, Victor Cionca, and Dirk Pesch. 2020. *FREE*—Fine-grained scheduling for reliable and energy-efficient data collection in LoRaWAN. *IEEE Internet of Things Journal* 7, 1 (2020), 669–683. DOI: http://dx.doi.org/10.1109/JIOT.2019.2949918
[26] William Hart Hayt, John A. Buck, et al. 1981. *Engineering Electromagnetics*, Vol. 6. McGraw-Hill, New York, NY.
[27] MSP 430 user guide. ([n. d.]). Retrieved from http://www.ti.com/lit/ug/slau445i/slau445i.pdf.
[28] Linx NT Series Transceiver User Guide. ([n. d.]). Retrieved from https://linxtechnologies.com/wp/wp-content/uploads/trm-fff-nt.pdf.
[29] TI CC1125 datasheet. ([n. d.]). Retrieved from http://www.ti.com/lit/ds/symlink/cc1125.pdf.
[30] USRP B200. ([n. d.]). Retrieved from https://www.ettus.com/all-products/ub200-kit/.
[31] Gregory J. Pottie and William J. Kaiser. 2000. Wireless integrated network sensors. *Communications of the ACM* 43, 5 (2000), 51–58.
[32] Vijay Raghunathan, Curt Schurgers, Sung Park, and Mani B. Srivastava. 2002. Energy-aware wireless microsensor networks. *IEEE Signal Processing Magazine* 19, 2 (2002), 40–50.
[33] Giuseppe Anastasi, Marco Conti, Mario Di Francesco, and Andrea Passarella. 2009. Energy conservation in wireless sensor networks: A survey. *Ad hoc Networks* 7, 3 (2009), 537–568.
[34] Tifenn Rault, Abdelmadjid Bouabdallah, and Yacine Challal. 2014. Energy efficiency in wireless sensor networks: A top-down survey. *Computer Networks* 67, 4 (2014), 104–122.
[35] Ridha Soua and Pascale Minet. 2011. A survey on energy efficient techniques in wireless sensor networks. In *Proceedings of the 2011 4th Joint IFIP Wireless and Mobile Networking Conference*. IEEE, 1–9.
[36] Gang Lu, Bhaskar Krishnamachari, and Cauligi S. Raghavendra. 2004. An adaptive energy-efficient and low-latency MAC for data gathering in wireless sensor networks. In *Proceedings of the18th International Parallel and Distributed Processing Symposium*. IEEE, 224.
[37] Ilker Demirkol, Cem Ersoy, and Fatih Alagoz. 2006. MAC protocols for wireless sensor networks: A survey. *IEEE Communications Magazine* 44, 4 (2006), 115–121.
[38] Wei Ye, John Heidemann, and Deborah Estrin. 2004. Medium access control with coordinated adaptive sleeping for wireless sensor networks. *IEEE/ACM Transactions on Networking* 12, 3 (2004), 493–506.
[39] Andrea Goldsmith. 2005. *Wireless Communications*. Cambridge University Press.
[40] Injong Rhee, Ajit Warrier, Mahesh Aia, Jeongki Min, and Mihail L. Sichitiu. 2008. Z-MAC: A hybrid MAC for wireless sensor networks. *IEEE/ACM Transactions on Networking* 16, 3 (2008), 511–524.
[41] Naoto Kimura and Shahram Latifi. 2005. A survey on data compression in wireless sensor networks. In *Proceedings of the International Conference on Information Technology: Coding and Computing*. Vol. 2, IEEE, 8–13.
[42] David Chu, Amol Deshpande, Joseph M. Hellerstein, and Wei Hong. 2006. Approximate data collection in sensor networks using probabilistic models. In *Proceedings of the 22nd International Conference on Data Engineering*. IEEE, 48–48.
[43] Bhargav Kanagal and Amol Deshpande. 2008. Online filtering, smoothing and probabilistic modeling of streaming data. In *Proceedings of the 2008 IEEE 24th International Conference on Data Engineering*. IEEE, 1160–1169.
[44] Aria Nosratinia, Todd E. Hunter, and Ahmadreza Hedayat. 2004. Cooperative communication in wireless networks. *IEEE Communications Magazine* 42, 10 (2004), 74–80.
[45] Zhong Zhou, Shengli Zhou, Shuguang Cui, and Jun-Hong Cui. 2008. Energy-efficient cooperative communication in a clustered wireless sensor network. *IEEE Transactions on Vehicular Technology* 57, 6 (2008), 3618–3628.

[46] Paolo Casari, Alessia Marcucci, Michele Nati, Chiara Petrioli, and Michele Zorzi. 2005. A detailed simulation study of geographic random forwarding (GeRaF) in wireless sensor networks. In *Proceedings of the 2005 IEEE Military Communications Conference*. IEEE, 59–68.
[47] Jamal N. Al-Karaki and Ahmed E. Kamal. 2004. Routing techniques in wireless sensor networks: A survey. *IEEE Wireless Communications* 11, 6 (2004), 6–28.
[48] Vamsi Paruchuri, Shivakumar Basavaraju, Arjan Durresi, Rajgopal Kannan, and S. Sitharama Iyengar. 2004. Random asynchronous wakeup protocol for sensor networks. In *Proceedings of the 1st International Conference on Broadband Networks*. IEEE.
[49] IEEE Standard 802.15.4. ([n. d.]). Retrieved from https://standards.ieee.org/standard/802_15_8-2017.html.
[50] Benjie Chen, Kyle Jamieson, Hari Balakrishnan, and Robert Morris. 2002. Span: An energy-efficient coordination algorithm for topology maintenance in ad hoc wireless networks. *Wireless Networks* 8, 5 (2002), 481–494.
[51] M. S. Trotter and G. D. Durgin. 2010. Survey of range improvement of commercial RFID tags with power optimized waveforms. In *Proceedings of the 2010 IEEE International Conference on RFID*. IEEE, 195–202.
[52] Mehran Abolhasan, Tadeusz Wysocki, and Eryk Dutkiewicz. 2004. A review of routing protocols for mobile ad hoc networks. *Ad Hoc Networks* 2, 1 (2004), 1–22.
[53] Vikram Iyer, Rajalakshmi Nandakumar, Anran Wang, Sawyer Fuller, and Shyamnath Gollakota. 2018. Living IoT: A flying wireless platform on live insects. arXiv:1812.09419. Retrieved from https://arxiv.org/abs/1812.09419.
[54] Evşen Yanmaz, Saeed Yahyanejad, Bernhard Rinner, Hermann Hellwagner, and Christian Bettstetter. 2018. Drone networks: Communications, coordination, and sensing. *Ad Hoc Networks* 68 (2018), 1–15.
[55] Rapeepat Ratasuk, Nitin Mangalvedhe, Yanji Zhang, Michel Robert, and Jussi-Pekka Koskinen. 2016. Overview of narrowband IoT in LTE Rel-13. In *Proceedings of the 2016 IEEE Conference on Standards for Communications and Networking*. IEEE, 1–7.
[56] Zigbee 3.0. ([n. d.]). Retrieved from https://www.nxp.com/products/wireless/zigbee/zigbee/zigbee-3.0:ZIGBEE-3-0.
[57] John R. Klauder, A. C. Price, Sidney Darlington, and Walter J. Albersheim. 1960. The theory and design of chirp radars. *Bell System Technical Journal* 39, 4 (1960), 745–808.
[58] Theodore S. Rappaport et al. 1996. *Wireless Communications: Principles and Practice*, Vol. 2. Prentice Hall PTR, New Jersey.
[59] MSP 430 FR2355. ([n. d.]). Retrieved from http://www.ti.com/product/MSP430FR2353.
[60] STM32L151x6. ([n. d.]). Retrieved from https://www.st.com/resource/en/datasheet/cd00277537.pdf.
[61] TI CC1101 datasheet. ([n. d.]). Retrieved from www.ti.com/lit/gpn/cc1101.
[62] Long-range RF communication:. ([n. d.]). Retrieved from http://www.ti.com/lit/wp/swry006/swry006.pdf.
[63] Matthew Gast. 2005. *802.11 Wireless Networks: The Definitive Guide*. O'Reilly Media, Inc.
[64] Kais Mekki, Eddy Bajic, Frederic Chaxel, and Fernand Meyer. 2019. A comparative study of LPWAN technologies for large-scale IoT deployment. *ICT Express* 5, 1 (2019), 1–7.
[65] Chuhan Gao, Mehrdad Hessar, Krishna Chintalapudi, and Bodhi Priyantha. 2019. Blind distributed MU-MIMO for IoT networking over VHF narrowband spectrum. In *Proceedings of the International Conference on Mobile Computing and Networking*. ACM.
[66] Cory Beard and William Stallings. 2015. *Wireless Communication Networks and Systems*. Pearson Education.
[67] Pei Huang, Li Xiao, Soroor Soltani, Matt W. Mutka, and Ning Xi. 2013. The evolution of MAC protocols in wireless sensor networks: A survey. *IEEE Communications Surveys & Tutorials* 15, 1 (2013), 101–120.
[68] James F. Kurose and Keith W. Ross. 2012. *Computer Networking: A Top-Down Approach* (6th ed.). Pearson.
[69] LoRa Airtime Calculator. ([n. d.]). Retrieved from https://www.loratools.nl/#/airtime.
[70] 32 kHz crystal oscillator. ([n. d.]).
[71] Ultra-Small Low Power, Low-Jitter, 1 Hz to 2.5 MHz Oscillator. ([n. d.]). Retrieved from https://www.sitime.com/products/1-hz-2-mhz-oscillatorstcxo/sit1579.
[72] Bernhard Korte, Jens Vygen, B. Korte, and J. Vygen. 2012. *Combinatorial Optimization*. Vol. 2, Springer.
[73] Open Source LoRa receiver. ([n. d.]). Retrieved from https://github.com/rpp0/gr-lora.
[74] Adafruit Feather 32u4 Radio. ([n. d.]). Retrieved from https://www.adafruit.com/product/3076.
[75] LoRa. ([n. d.]). Retrieved from https://www.semtech.com/products/wireless-rf/lora-transceivers/sx1272.
[76] Floris Van den Abeele, Ingrid Moerman, Jeroen Hoebeke, and Jetmir Haxhibeqiri. (n. d.). LoRa scalability: A simulation model based on interference measurements. *Sensors* 16, 6.
[77] Venkat Anantharam and Sergio Verdu. 1996. Bits through queues. *IEEE Transactions on Information Theory*, 42, 1 (1996), 4–18.
[78] Anand S. Bedekar and Murat Azizoglu. 1998. The information-theoretic capacity of discrete-time queues. *IEEE Transactions on Information Theory* 44, 2 (1998), 446–461.
[79] Rajesh Sundaresan and Sergio Verdú. 2000. Robust decoding for timing channels. *IEEE Transactions on information Theory* 46, 2 (2000), 405–419.

[80] Rajesh Sundaresan and Sergio Verdú. 2006. Capacity of queues via point-process channels. *IEEE/ACM Transactions on Networking* 14, SI (2006), 2697–2709.
[81] Balaji Prabhakar and Robert Gallager. 2003. Entropy and the timing capacity of discrete queues. *IEEE Transactions on Information Theory* 49, 2 (2003), 357–370.
[82] Sarah H. Sellke, C.-C. Wang, Saurabh Bagchi, and Ness Shroff. 2009. TCP/IP timing channels: Theory to implementation. In *Proceedings of the IEEE INFOCOM'09*. IEEE.
[83] Pandurang Kamat, Wenyuan Xu, Wade Trappe, and Yanyong Zhang. 2009. Temporal privacy in wireless sensor networks: Theory and practice. *ACM Transactions on Sensor Networks* 5, 4 (2009), 28.
[84] Wenyuan Xu, Wade Trappe, and Yanyong Zhang. 2008. Anti-jamming timing channels for wireless networks. In *Proceedings of the 1st ACM Conference on Wireless Network Security*. ACM, 203–213.
[85] Yujie Zhu and Raghupathy Sivakumar. 2005. Challenges: Communication through silence in wireless sensor networks. In *Proceedings of the 11th Annual International Conference on Mobile Computing and Networking*. ACM, 140–147.
[86] Da-shan Shiu and Joseph M. Kahn. 1999. Differential pulse-position modulation for power-efficient optical communication. *IEEE Transactions on Communications* 47, 8 (1999), 1201–1210.
[87] Zabih Ghassemlooy, A. R . Hayes, N. L. Seed, and E. D. Kaluarachchi. 1998. Digital pulse interval modulation for optical communications. *IEEE Communications Magazine* 36, 12 (1998), 95–99.
[88] Hisayoshi Sugiyama and Kiyoshi Nosu. 1989. MPPM: A method for improving the band-utilization efficiency in optical PPM. *Journal of Lightwave Technology* 7, 3 (1989), 465–472.
[89] Hyuncheol Park and J. R. Barry. 2004. Trellis-coded multiple-pulse-position modulation for wireless infrared communications. *IEEE Transactions on Communications* 52, 4 (April 2004), 643–651.
[90] Hyuncheol Park and J. R. Barry. 1995. Modulation analysis for wireless infrared communications. In *Proceedings of the IEEE International Conference on Communications*. Vol. 2, 1182–1186.
[91] Li Zhao and A. M. Haimovich. 2002. Multi-user capacity of M-ary PPM ultra-wideband communications. In *Proceedings of the 2002 IEEE Conference on Ultra Wideband Systems and Technologies*. 175–179.
[92] Li Zhao and A. M. Haimovich. 2001. Capacity of M-ary PPM ultra-wideband communications over AWGN channels. In *Proceedings of the IEEE Vehicular Technology Conference*.
[93] Zhi Zhang, Zhonghai Lu, Qiang Chen, Xiaolang Yan, and Li-Rong Zheng. 2012. Code division multiple access/pulse position modulation ultra-wideband radio frequency identification for Internet of Things: Concept and analysis. *International Journal of Communication Systems* 25, 9 (2012), 1103–1121.
[94] Francesca Cuomo and C. Martello. 2001. MAC principles for an ultra wide band wireless access. In *Proceedings of the IEEE Global Telecommunications Conference*.
[95] Xuemin Shen, Weihua Zhuang, Hai Jiang, and Jun Cai. 2005. Medium access control in ultra-wideband wireless networks. *IEEE Transactions on Vehicular Technology* 54, 5 (2005), 1663–1677.
[96] Dong Sam Ha and Patrick R. Schaumont. Replacing cryptography with ultra wideband modulation in secure RFID. In *Proceedings of the 2007 IEEE International Conference on RFID*.
[97] Z. Lin and P. Wei. 2006. Pulse position modulation time hopping ultra wideband sharing signal for radar and communication system. In *Proceedings of the 2006 CIE International Conference on Radar*. 1–4.
[98] R. Scholtz. 1993. Multiple access with time-hopping impulse modulation. In *Proceedings of the IEEE Military Communications Conference*.

Received 26 February 2022; revised 22 June 2022; accepted 8 July 2022